Fault-Tolerant Quantum Computation by Hybrid Qubits with Bosonic Cat Code and Single Photons

Jaehak Lee,[1,2] Nuri Kang,[1,3] Seok-Hyung Lee,[2,4] Hyunseok Jeong,[2] Liang Jiang,[5] and Seung-Woo Lee[1,*]

[1] *Center for Quantum Information, Korea Institute of Science and Technology (KIST), Seoul 02792, Korea*
[2] *Department of Physics and Astronomy, Seoul National University, Seoul 08826, Korea*
[3] *Department of Physics, Korea University, Seoul 02841, Korea*
[4] *Centre for Engineered Quantum Systems, School of Physics, The University of Sydney, Sydney, New South Wales 2006, Australia*
[5] *Pritzker School of Molecular Engineering, The University of Chicago, Chicago, Illinois 60637, USA*

(Received 17 January 2024; revised 19 April 2024; accepted 7 June 2024; published 2 August 2024; corrected 29 January 2025)

Hybridizing different degrees of freedom or physical platforms potentially offers various advantages in building scalable quantum architectures. Here, we introduce a fault-tolerant hybrid quantum computation by building on the advantages of both discrete-variable (DV) and continuous-variable (CV) systems. In particular, we define a CV-DV hybrid qubit with a bosonic cat code and a single photon, which is implementable in current photonic platforms. Due to the cat code encoded in the CV part, the predominant loss errors are readily correctable without multiqubit encoding, while the logical basis is inherently orthogonal due to the DV part. We design fault-tolerant architectures by concatenating hybrid qubits and an outer DV quantum error-correction code such as a topological code, exploring their potential merit in developing scalable quantum computation. We demonstrate by numerical simulations that our scheme is at least an order of magnitude more resource efficient compared to all previous proposals in photonic platforms, allowing us to achieve a record-high loss threshold among existing CV and hybrid approaches. We discuss the realization of our approach not only in all-photonic platforms but also in other hybrid platforms including superconducting and trapped-ion systems, which allows us to find various efficient routes toward fault-tolerant quantum computing.

DOI: 10.1103/PRXQuantum.5.030322

I. INTRODUCTION

In working toward fully fault-tolerant quantum computing, various physical platforms, such as photons [1–3], superconductors [4–6], trapped ions [7,8], nitrogen vacancies in diamond [9–11], and quantum dots [12,13], have been explored and considered as the building blocks for scalable quantum systems. Irrespective of the physical platforms, information is encoded into qubits defined with the basis in either discrete-variable (DV) [14–19] or continuous-variable (CV) [20–34] degrees of freedom, each of which has its own pros and cons. In recent years, hybrid approaches integrating different physical degrees of freedom to overcome the limitations of each platform have opened up a new paradigm in quantum technologies. Hybridization may be quite a natural direction for scalability, since each platform has its own advantage depending on the circumstances and it is frequently required to convert quantum information between different platforms [35–37]. In particular, various CV-DV hybrid protocols have recently been proposed [38–53] and experimentally demonstrated [54–63] to combine their advantages in quantum computing and quantum communications.

Meanwhile, qubits encounter errors due to interactions with the environment and imperfect operations, which accumulate and become more severe as the size of the system increases. Quantum error correction (QEC) provides systematic ways to protect qubits from the predominant errors [64,65] and allows us to achieve fault tolerance in building scalable quantum architectures. In QEC, information is typically encoded in a Hilbert space larger than a qubit space so that any error can be detected if it brings the encoded state out of the logical code space. By restoring the state back to the code space, errors can be corrected without compromising the encoding of

*Contact author: swleego@gmail.com

logical information. While multiple physical qubits of finite-dimensional systems are typically used to construct a single logical qubit in a DV code, a bosonic system characterized by an infinite-dimensional Hilbert space can provide a large number of degrees of freedom to encode a logical qubit in such a CV approach. Several bosonic error-correction codes, in which a qubit is defined in a single oscillator, have been proposed, such as the Gottesman-Kitaev-Preskill (GKP) [66], binomial [67] and the cat code [21–23,68–71]. These codes are elaborately designed, in particular, to protect against photon loss [72–74]. Recently, bosonic error-correction codes have been demonstrated and exploited for building quantum computing systems in various experimental platforms [75–96].

In this work, we introduce a hybrid quantum computing scheme by building on the advantages of both CV and DV systems toward fault-tolerant quantum computation. In particular, we define a logical qubit by hybridizing a cat-code-encoded state with a single photon. Due to the cat code encoded in the CV part, the effect of loss is readily correctable even without multiqubit encoding, while its logical basis is inherently orthogonal due to the DV part, in contrast to other CV qubits [21–23,64,68–71,97]. Such hybrid qubits can be experimentally generated in current photonic platforms [55,56,61,63]. We then design quantum computing architectures by concatenating the hybrid qubits and an outer DV quantum error-correction code, such as the Steane code [98] or the surface code [99–101]. Specifically, here we focus on all-photonic implementations for direct comparison with previous proposals [15,16,41,50,102]. To that end, we define hybrid-fusion schemes, which are implementable in current experimental platforms with linear optics, as building blocks for scalable architectures [55,56]. We then numerically simulate and analyze the fault tolerance of our hybrid scheme, showing that it is at least an order of magnitude more resource efficient compared to all previous proposals in photonic platforms, owing to the use of the bosonic cat code in the physical level. Moreover, it is demonstrated that our scheme allows us to achieve at least 4-times-higher loss thresholds compared to existing hybrid and CV approaches [41,50,102]. We stress that our scheme is not limited to all-photonic platforms but can be implementable in other hybrid platforms, including superconducting [75–78,103–107] and trapped-ion systems [62,81,108–114], which thus allows us to find various routes toward scalable fault-tolerant quantum computing.

II. HYBRID QUBITS FOR QUANTUM COMPUTATION

A. Hybrid qubit

We define a hybrid qubit by employing a single-photon (DV qubit) and a cat-code-encoded state (CV qubit), which we call the hybrid cat-code (H-cat) qubit. The cat code is a bosonic QEC code designed to protect qubits against photon loss, in which qubits are encoded in the subspace of even-photon-number states, so that a photon loss can be detected when the parity changes [68,69]. Specifically, the code space is defined by even cat states $\{|\mathcal{C}_\alpha^+\rangle, |\mathcal{C}_{i\alpha}^+\rangle\}$, where $|\mathcal{C}_\alpha^+\rangle = \mathcal{N}_\mathcal{C}^+(|\alpha\rangle + |-\alpha\rangle)$ with the normalization factor $\mathcal{N}_\mathcal{C}^+ \equiv 1/\sqrt{2(1+e^{-2\alpha^2})}$ and $|\alpha\rangle$ is a coherent state with amplitude α. By combining DV and CV qubits, the basis of the H-cat qubit can then be defined as

$$\left\{|0_L\rangle = |+\rangle|\mathcal{C}_\alpha^+\rangle, |1_L\rangle = |-\rangle|\mathcal{C}_{i\alpha}^+\rangle\right\}, \tag{1}$$

where $|\pm\rangle = (|H\rangle \pm |V\rangle)/\sqrt{2}$ is the polarization of a single photon. Note that the logical bases are orthogonal to each other due to the DV part, in contrast to the bases $\{|\mathcal{C}_\alpha^+\rangle, |\mathcal{C}_{i\alpha}^+\rangle\}$ in bosonic quantum computation, which overlap each other with finite α and cause inherent errors. We also consider another type of hybrid qubit [41] for comparison, composed of a single photon and a coherent state in the basis $\{|+\rangle|\alpha\rangle, |-\rangle|-\alpha\rangle\}$, which we call here the hybrid coherent-state (H-coh) qubit. The hybrid qubits, i.e., H-cat and H-coh, are illustrated in Fig. 1(a).

Note that hybrid qubits can be generated in current photonic platforms. CV-DV hybrid entangled states have been experimentally demonstrated in optical systems [55,56] and successfully applied to quantum computing and communications in numerous experiments [48,61,63]. In those experiments, the CV basis is defined by coherent states,

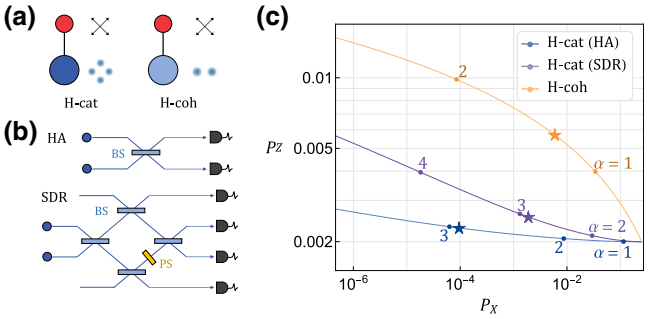

FIG. 1. (a) An illustration of the hybrid qubits. In our H-cat qubit, DV (red) and CV (blue) qubits are encoded, respectively, in the polarization degree of freedom and in the even cat states $\{|\mathcal{C}_\alpha^+\rangle, |\mathcal{C}_{i\alpha}^+\rangle\}$, while the CV qubit is encoded in the coherent states (light blue) in the H-coh qubit. (b) Schemes for the fusion operations of CV qubits. We employ two separate schemes of cat-code Bell measurement, which we refer to as the HA scheme [115] and the SDR scheme [116], respectively. BS and PS represent a beam splitter and a $\pi/2$ phase shifter, respectively. (c) The error rates P_X and P_Z for the fusion of hybrid qubits under loss rate $\eta = 2 \times 10^{-3}$. The orange curve is for the H-coh scheme and the blue (purple) curve is for the H-cat scheme, employing the HA (SDR) scheme. The numbers indicated at each point represent the corresponding amplitude α. The points marked as stars represent the optimal encoding amplitude α, which achieves the highest loss threshold.

i.e., $|\alpha\rangle$ and $|-\alpha\rangle$, constituting two-component cat states in the CV part, so that the generated hybrid entangled states can be directly used as the H-coh qubit by means of simple modifications. We can also generate the H-cat qubit by using H-coh qubits by extending two-component cat states into four-component cat states using $|\alpha\rangle$, $|i\alpha\rangle$, $|-\alpha\rangle$, and $|-i\alpha\rangle$ in the CV part, e.g., using two H-coh qubits, a beam splitter, and a photon-number-resolving (PNR) detector, as proposed in Ref. [117]. We present the scheme for H-cat-qubit generation in Sec. IV A.

We stress that such CV-DV hybrid entanglement can also be generated efficiently in other platforms, including superconducting and trapped-ion systems, which enables our approach to be more generally implemented in any CV-DV hybrid platform for quantum computing. We discuss these implementations further in Sec. IV B.

B. Hybrid fusion

We now introduce a *hybrid fusion*, i.e., a CV-DV hybrid entangling operation, which is performed by the joint work of Bell-state measurements on CV and DV qubits. A fusion measurement is typically applied on entangled states to generate larger-size entangled states such as cluster states as prerequisites for measurement-based quantum computation (MBQC) [93,118,119] or also to enable universal gate operations via teleportation in circuit-based quantum computation [120].

A hybrid-fusion operation projects a two hybrid qubits on one of the hybrid Bell states $|\Psi_L^{\pm}\rangle = (|0_L\rangle|1_L\rangle \pm |1_L\rangle|0_L\rangle)/\sqrt{2}$ and $|\Phi_L^{\pm}\rangle = (|0_L\rangle|0_L\rangle \pm |1_L\rangle|1_L\rangle)/\sqrt{2}$. The logical Bell states of the hybrid qubits given in the basis of Eq. (1) can be rewritten by separating the CV and DV parts as (for details, see Appendix A 1)

$$\begin{aligned} |\Psi_L^{\pm}\rangle &\propto |\Phi_{\mathcal{D}}^{-}\rangle|\tilde{\Psi}_{\mathcal{C}}^{\pm}\rangle + |\Psi_{\mathcal{D}}^{-}\rangle|\tilde{\Psi}_{\mathcal{C}}^{\mp}\rangle, \\ |\Phi_L^{\pm}\rangle &\propto |\Phi_{\mathcal{D}}^{+}\rangle|\tilde{\Phi}_{\mathcal{C}}^{\pm}\rangle + |\Psi_{\mathcal{D}}^{+}\rangle|\tilde{\Phi}_{\mathcal{C}}^{\mp}\rangle, \end{aligned} \tag{2}$$

where $|\Psi_{\mathcal{D}}^{\pm}\rangle = (|H\rangle|V\rangle \pm |V\rangle|H\rangle)/\sqrt{2}$, $|\Phi_{\mathcal{D}}^{\pm}\rangle = (|H\rangle|H\rangle \pm |V\rangle|V\rangle)/\sqrt{2}$ are the Bell states of the DV qubits, and $|\tilde{\Psi}_{\mathcal{C}}^{\pm}\rangle = |\mathcal{C}_{\alpha}^{+}\rangle|\mathcal{C}_{i\alpha}^{+}\rangle \pm |\mathcal{C}_{i\alpha}^{+}\rangle|\mathcal{C}_{\alpha}^{+}\rangle$ and $|\tilde{\Phi}_{\mathcal{C}}^{\pm}\rangle = |\mathcal{C}_{\alpha}^{+}\rangle|\mathcal{C}_{\alpha}^{+}\rangle \pm |\mathcal{C}_{i\alpha}^{+}\rangle|\mathcal{C}_{i\alpha}^{+}\rangle$ are the unnormalized Bell states of the CV qubits.

Therefore, the hybrid-fusion operation can be implemented by applying CV and DV Bell-state measurements—denoted here as $B_{\mathcal{C}}$ and $B_{\mathcal{D}}$, respectively—separately. Its logical outcome can then be discriminated by combining the results of $B_{\mathcal{C}}$ and $B_{\mathcal{D}}$ based on Eq. (2). $B_{\mathcal{C}}$ can be implemented by linear optics and PNR detectors, as illustrated in Fig. 1(b). Two schemes have recently been independently proposed in Refs. [115,116]; we refer to them as the HA and SDR scheme, respectively (for details, see Appendix A 2). $B_{\mathcal{C}}$ can discriminate the Bell states through the pattern of the measurement outcomes as denoted in the tables of Figs. 4(b) and 4(c); while the logical $+/-$ sign of Bell states can be distinguished with certainty by counting the total number of photons detected, there exists ambiguity in discriminating the logical letter Ψ or Φ for some measurement outcomes, to which we assign the X error with rate p_X.

In our hybrid scheme, we can remove the ambiguity through the use of $B_{\mathcal{D}}$. In the photon-polarization encoding, $B_{\mathcal{D}}$ can be chosen as a so-called type-II fusion [14] that distinguishes two Bell states $|\Psi_{\mathcal{D}}^{\pm}\rangle$ out of four with linear optics [121,122] (see Appendix A 3). Once $B_{\mathcal{D}}$ succeeds, it removes the ambiguity between the letters Ψ and Φ. Remarkably, a hybrid-fusion operation is thus able to distinguish hybrid Bell states with certainty even if only one of $B_{\mathcal{C}}$ and $B_{\mathcal{D}}$ succeeds. Otherwise—i.e., in the case in which $B_{\mathcal{C}}$ yields ambiguity and $B_{\mathcal{D}}$ fails—the resulting state after the hybrid fusion can be represented by $\mu|\Phi_L^{\pm}\rangle + \nu|\Psi_L^{\pm}\rangle$. So, when $|\mu| \geq |\nu|$, we can take $|\Phi_L^{\pm}\rangle$ as the outcome and assign an X error with rate $P_X = |\nu|^2/(|\mu|^2 + |\nu|^2)$ and vice versa. We calculate the X error rate of hybrid fusion employing the HA or SDR scheme as described in Appendix A.

Moreover, in the presence of photon loss, $B_{\mathcal{C}}$ can detect a single-photon loss in the CV part through detecting the parity change of the cat state to odd, i.e., when a total odd number of photons is detected. This is due to the bosonic cat-code error correction in the CV part. The hybrid-fusion operation can thus successfully yield an outcome that contains an X error with a rate that is slightly changed from P_X (see Appendix A 2). If two or more photons are lost, the Z errors remain undetected in the fusion-measurement outcome, as we analyze in Sec. II C.

C. Error analysis

If more than one photon is lost, the errors can be modeled by applying higher powers of $\hat{a}$. In the CV part, the cat code exhibits a cyclic behavior [70], i.e., the state after $4k + l$ photon loss has the same form as the state after l photon loss, where k is a nonnegative integer and $l = 0, 1, 2, 3$. Since each photon loss induces a parity change, the CV qubit is in even (odd) space when l is even (odd). A Z error may occur by multiple-photon loss, as $B_{\mathcal{C}}$ only corrects single-photon loss detected by the parity change. If two photons are lost ($l = 2$) at one input port, a Z error occurs as $\hat{a}^2(a|\mathcal{C}_{\alpha}^{+}\rangle + b|\mathcal{C}_{i\alpha}^{+}\rangle) = (a|\mathcal{C}_{\alpha}^{+}\rangle - b|\mathcal{C}_{i\alpha}^{+}\rangle)$ and it remains undetected because there is no parity change. When one photon is lost from each CV input port, the total photon number is even but the parity change may be distinguishable by some measurement patterns (see Appendix A 2), which themselves cause no error. If the parity change is not distinguishable, a Z error remains undetected. If $l = 3$, only single-photon loss is corrected and thus a Z error remains uncorrected as in the case of $l = 2$. For the case of higher photon loss, we can make a

similar error analysis and we summarize it in Appendix C. On the other hand, if any DV photons are lost, we lose the phase information, which causes a dephasing error. DV-photon loss is locatable by counting the total number of photons detected in $B_{\mathcal{D}}$. To sum up, we denote P_Z to be the overall Z error rate induced by photon loss. We derive the explicit expressions for the X error rate P_X and the Z error rate P_Z in Appendix C.

In Fig. 1(c), we present the X and Z error rates under loss for the hybrid fusions. Specifically, P_X and P_Z are plotted for the fusions of H-cat qubits with HA and SDR, and the H-coh qubit used in Ref. [41,50,51], by varying the amplitude α under a fixed loss rate $\eta = 2 \times 10^{-3}$. This shows that the effect of loss can be substantially suppressed in the hybrid fusion of the H-cat compared to the H-coh due to the bosonic cat-code error correction in the CV part. As common tendencies, the P_X error can be exponentially suppressed as α grows because the basis of the CV part is more distinguishable, while P_Z only increases linearly with $|\alpha|^2$ because its state becomes more fragile against photon loss. The result clearly shows that P_Z is suppressed by employing the cat-code error correction. By taking a larger encoding amplitude α, we can always achieve much smaller P_X and P_Z in the fusions of H-cat qubits than H-coh qubits. By comparing two different types of fusion schemes of H-cat qubits, i.e., HA and SDR, the HA scheme exhibits lower error rates, whereas we show that the SDR scheme is advantageous when an unambiguous discrimination is required without error (see Appendix A 2).

III. FAULT-TOLERANT QUANTUM COMPUTATION

A. Hybrid quantum computing architectures

Let us now design quantum computing architectures based on the hybrid qubits. We can consider both the circuit-based and MBQC models. In the circuit-based model, the gate operations for universal quantum computation can be chosen as the gate set $\{\hat{X}, \hat{Z}_\theta, \hat{H}, \hat{\mathrm{CZ}}\}$. The Pauli-$X$ operation ($\hat{X}$) and arbitrary rotation along the Z axis ($\hat{Z}_\theta$) are implementable only using linear optical elements; $\hat{X}$ can be implemented by applying bit-flip operations in both the CV and the DV parts, using a polarization rotator acting as $|+\rangle \leftrightarrow |-\rangle$ and a $\pi/2$ phase shifter acting as $|\mathcal{C}_\alpha^+\rangle \leftrightarrow |\mathcal{C}_{i\alpha}^+\rangle$. $\hat{Z}_\theta$ can be implemented by a θ phase shifter applied only as $|-\rangle \to e^{i\theta}|-\rangle$ on the DV part. The Hadamard ($\hat{H}$) and controlled-Z ($\hat{\mathrm{CZ}}$) gates can be performed based on the gate-teleportation technique [120], using the hybrid-fusion scheme and entangled resource states. The resource states as the channel of teleportation for $\hat{H}$ and $\hat{\mathrm{CZ}}$ are given, respectively, by $|\Phi_H\rangle \propto |0_L, 0_L\rangle + |0_L, 1_L\rangle + |1_L, 0_L\rangle - |1_L, 1_L\rangle$ and $|\Phi_{\mathrm{CZ}}\rangle \propto |0_L, 0_L, 0_L, 0_L\rangle + |0_L, 0_L, 1_L, 1_L\rangle + |1_L, 1_L, 0_L, 0_L\rangle - |1_L, 1_L, 1_L, 1_L\rangle$. We present the scheme for resource-state generation in Sec. IV A. The measurement in the Z basis can be performed by the measurement in the DV part using polarization measurement (for details of the schemes of hybrid teleportation and measurement, see Appendix B).

Constructing a fault-tolerant architecture in our hybrid approach requires us to concatenate the hybrid qubits incorporating the bosonic cat code and an outer DV quantum error-correction code such as the Calderbank-Shor-Steane (CSS) [98] and topological codes [99–101]. For a direct comparison with previous works [15,16,41,50,102], we construct a circuit-based fault-tolerant model using the seven-qubit Steane code (see Appendix D), while we employ the surface code for MBQC as described below.

In MBQC, we construct a Raussendorf-Harrington-Goya (RHG) lattice embedding the surface code as shown in Fig. 2(a). We first prepare three-qubit micro cluster states by using hybrid qubits as element resources, as we describe in Sec. IV A, which we refer to as three-qubit micro *H-cluster* states. We then merge such micro H-cluster states using hybrid fusion to construct an RHG lattice. In step 1, three micro H-cluster states are merged by two hybrid fusions to form a five-qubit star H-cluster state with one central qubit and four side qubits. In step 2, we pile star H-cluster states in the form of an RHG lattice, where the central hybrid qubits become vertices of cluster states and the side qubits are consumed by hybrid fusion to create edges between adjacent vertices. We note that the deterministic nature of hybrid fusion enables a resource-efficient construction of the RHG lattice. Moreover, photon loss can be corrected to some extent by implementing the hybrid fusion so that higher loss thresholds can be reached, which we will discuss in Sec. III B.

In the RHG lattice, each x-y plane is called a layer and the t axis represents the simulated time. The size of the RHG lattice is characterized by the code distance d. A layer is primal (dual) if it is located at even (odd) t and primal (dual) qubits reside on faces (edges) of the primal lattice. The stabilizer of a primal unit cell is given by the product of six Pauli-X operations on primal qubits located on the faces. The error patterns matching the stabilizer measurement can be corrected and the remaining error chain connecting two primal boundaries causes a logical error. Note that here we only simulate Z errors in primal lattices, because error corrections are done separately on the primal and dual lattice and qubits are measured in the X basis for stabilizer measurements.

B. Fault-tolerance analysis

We investigate the fault tolerance of quantum computation with H-cat and H-coh qubits and compare the result with previous works. Here, we focus on analyzing and simulating the fault tolerance of MBQC, which is suitable for photonic platforms. For the circuit-based model, we employ the telecorrection [128] and the Steane code

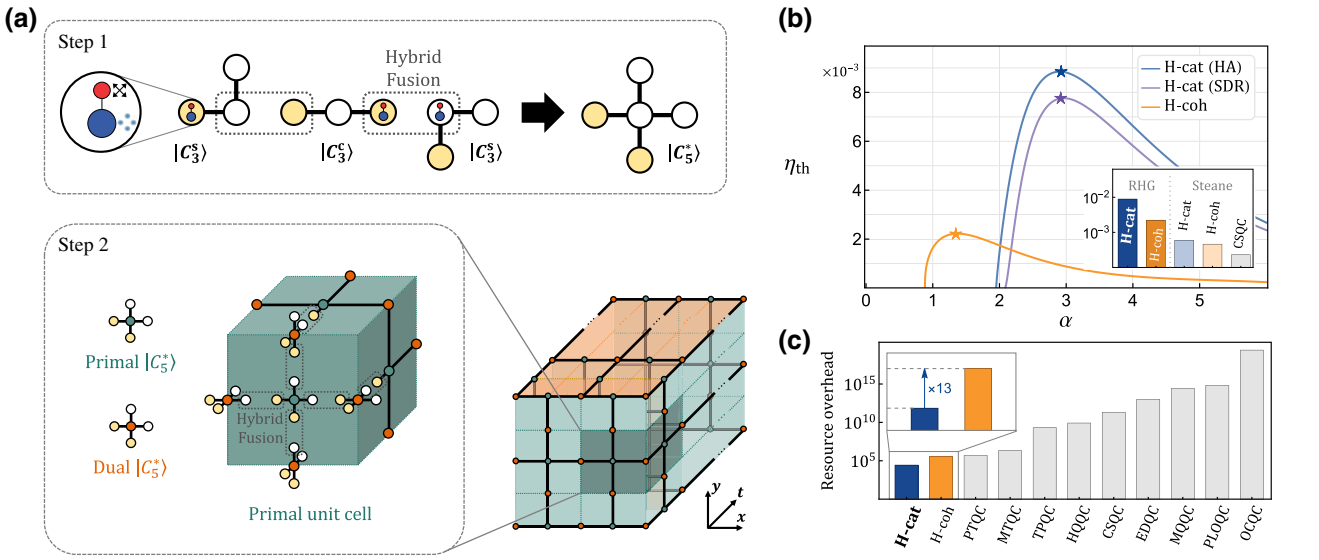

FIG. 2. (a) A schematic to build an RHG lattice by means of hybrid qubits. Step 1: one central micro H-cluster state $|C_3^c\rangle$ and two side micro H-cluster states $|C_3^s\rangle$ are merged using two hybrid fusions to create a star H-cluster state $|C_5^*\rangle$. The micro cluster states differ by Hadamard gates, which are applied on the qubits shaded with yellow, from typical cluster states. Step 2: in a unit cell of an RHG lattice, qubits are located at each face and edge. Star H-cluster states are placed on each location and merged by hybrid fusion on side qubits. (b) The loss thresholds obtained by simulation in an RHG lattice with different schemes. Points marked as stars represent the highest loss threshold. The inset represents the comparison of optimal thresholds, including previous approaches with the Steane code. (c) A comparison of the resource overheads of existing photonic quantum computing proposals to achieve the logical error rate $p_L = 10^{-6}$. Hybrid quantum computing with H-cat qubits requires 13 times less resource compared to H-coh qubits when the H-coh pair is chosen to be the common resource state. We also compare with other existing photonic schemes: parity-encoding-based topological quantum computing (PTQC) [123], multiphoton-qubit-based topological quantum computing (MTQC) [124], topological photonic quantum computing (TPQC) [16], hybrid-qubit-based quantum computing (HQQC) [41], coherent-state quantum computing (CSQC) [102], error-detecting quantum state transfer (EDQC) [125], multiphoton qubit quantum computing (MQQC) [126], parity-state linear optical quantum computing (PLOQC) [127], and optical cluster-state quantum computing (OCQC) [15].

in simulation equivalently with the works using H-coh and CV qubits [41,102] for a direct comparison, details of which are presented in Appendix D.

In the RHG lattice, errors that occur in the hybrid fusion propagate to adjacent qubits (see Appendix C 3), so that a corresponding error rate is assigned to each individual qubit on the lattice. Based on assigned error rates, we can find the error pattern matching the syndrome measurement using weighted minimum-weight perfect matching [129] in the PyMatching package [130] and then count remaining error chains connecting two primal boundaries and determine whether a logical error occurs. We perform a Monte Carlo simulation to find the logical error rate p_L for different code distances d and then investigate whether the errors are accumulated, i.e., p_L increases or not with increasing d. The fault-tolerance noise thresholds can then be determined as the maximum physical error rates by which the logical errors are not accumulated with d (for details, see Appendix D).

We present the loss thresholds of photonic MBQC based on H-cat and H-coh qubits in Fig. 2(b) by changing the encoding amplitude α in the CV part. Note that the previous estimation of H-coh in Ref. [50] has employed a slightly different error model and thus we resimulate the result under the same error model assigned to H-cat for a fair comparison. We also depict the loss thresholds of the circuit-based model with hybrid and CV qubits estimated based on Steane codes for comparison.

This shows that hybrid MBQC with H-cat qubits achieves the highest loss thresholds compared to other approaches including MBQC with H-coh qubits as well as all hybrid and CV approaches in circuit-based models. The loss threshold of quantum computing with the H-cat, 0.89%, is about 4 times larger than the maximum 0.22% estimated with the H-coh [50]. Hybrid fusion with the HA scheme yields a higher threshold than the SDR scheme, as the former exhibits lower error rates than the latter.

The highest thresholds can be reached by an optimized encoding of α marked by stars in Figs. 2(b) and 1(c); $\alpha \approx 2.93$ for the H-cat with the HA scheme and $\alpha \approx 1.37$ for H-coh qubits. The threshold curves of the H-cat and H-coh qubits show a common tendency in that they rapidly increase up to the peak and decrease gradually. This is because enlarging the encoding amplitude α can reduce P_X but enhance P_Z, so that at some point further increase of α eventually degrades the thresholds. As exhibited in

Fig. 1(c), the enhancement of the loss thresholds can be achieved with H-cat qubits, as P_X can be significantly reduced further while suppressing P_Z by increasing α, due to the inherent bosonic error correction in the CV part.

C. Resource overhead

To investigate the resource overhead, we estimate the number of unit resources, referred to as $\mathcal{N}_{p_L}$, to achieve the target logical error rate p_L. We choose the H-coh pair as a unit resource for a fair comparison with the resource estimation in previous works [41,50]. We propose a scheme to generate an H-cat pair consuming eight H-coh pairs as illustrated in Fig. 3(a), details of which are also explained in Sec. IV A. Two H-coh pairs can be merged by applying B_{I} on DV and beam-splitter interaction followed by photon-number counting on CV qubits. The resulting state can be postselected with a probability of approximately $1/4$ of obtaining an H-cat pair. Thus, here we estimate that an H-cat pair is 8 times as expensive as an H-coh pair.

We find that with H-cat qubits, a target logical error rate can be achieved even with a very small code distance d. For example, to achieve $p_L = 10^{-6}$, only $d = 4$ is sufficient with H-cat qubits, due to the suppressed errors caused by the bosonic cat code in the CV part of the physical level, while $d = 15$ is required with H-coh qubits [50]. As a result, we can estimate that the resource overhead for the hybrid MBQC with H-cat qubits is $\mathcal{N}_{10^{-6}} = 2.7 \times 10^4$, which is 13 times more efficient compared to the overhead for the MBQC with H-coh qubits, $\mathcal{N}_{10^{-6}} = 3.6 \times 10^5$. Remarkably, employing H-cat qubits can reduce the resource cost by an order of magnitude compared to the approach with H-coh qubits.

In Fig. 2(c), we present the resource-cost estimation of the proposed hybrid quantum computing schemes with H-cat and H-coh qubits. We also compare the resource efficiencies of the proposed schemes with existing MBQC photonic schemes based on direct encoding [16], repetition codes [124], and parity encoding of multiple photons [123], as well as circuit-based photonic schemes [15,102,125–127] (for resource analysis of other schemes, see Refs. [51,124]). This shows that our hybrid approach is at least an order of magnitude more resource efficient compared to all the other photonic proposals with respect to the cost of the resources, while the direct comparison is not straightforward due to the different types of resource states. The improved resource efficiency is achieved in our scheme due to the deterministic nature of the proposed hybrid fusion and the loss tolerance of the resource states due to the inherently encoded bosonic cat code.

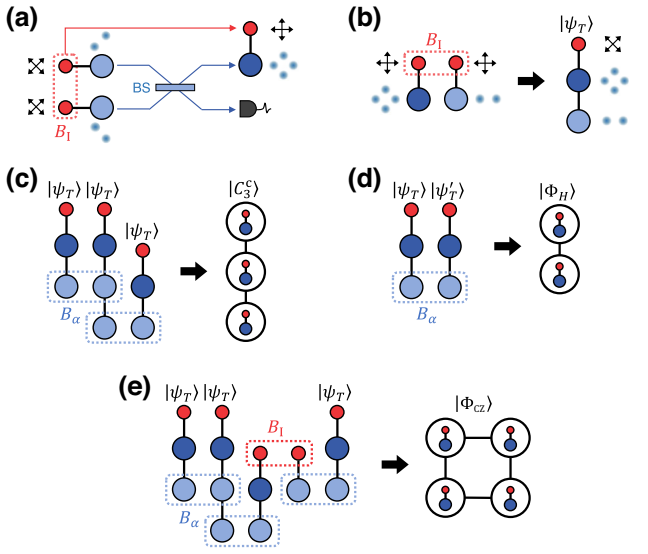

FIG. 3. (a) Generation scheme of an H-cat pair. Red circles represent DV qubits and its polarization bases are represented as arrows. Blue circles represent cat-code qubits using four components of coherent states and light blue circles represent coherent-state qubits using two components of coherent states. (b) Generation scheme of a DV-coherent-cat triple $|\psi_T\rangle$. Another type of triple $|\psi_T'\rangle$ can be obtained by rotating the DV basis of H-coh pair from H/V to $+/-$. By merging hybrid triples and hybrid pairs, we can generate off-line resource states such as (c) three-qubit H-cluster state $|C_3^c\rangle$, (d) Hadamard resource $|\Phi_H\rangle$, and (e) CZ resource $|\Phi_{\mathrm{CZ}}\rangle$.

IV. PHYSICAL IMPLEMENTATIONS

A. Resource-state generation

We introduce an H-coh pair $(|+\rangle|\alpha\rangle + |-\rangle|-\alpha\rangle)/\sqrt{2}$, which is employed as a logical qubit in previous hybrid approaches [41,50], as a unit resource. It can be prepared by the scheme of Refs. [56,61,63], where DV-CV entanglement is heralded by the detection of a single photon after a weak beam-splitter interaction between the CV and DV modes. Since this scheme employs the CV basis using two coherent states, $|\alpha\rangle$ and $|-\alpha\rangle$, we have to extend it to a four-component cat code using $|\alpha\rangle$, $|i\alpha\rangle$, $|-\alpha\rangle$, and $|-i\alpha\rangle$. The generation of a four-component cat state has been proposed in Ref. [117], where a pair of two-component cat states in different phases have been mixed by a beam-splitter interaction followed by photon-number counting on one of the output modes. Here, we propose the generation of an H-cat pair following the scheme described in Fig. 3(a). We begin with two H-coh pairs, $(|+\rangle|\omega\alpha\rangle + |-\rangle|-\omega\alpha\rangle) \otimes (|+\rangle|-i\omega\alpha\rangle + |-\rangle|i\omega\alpha\rangle)$, where $\omega = e^{i\pi/4}$. For convenience, we omit the normalization factors. The DV qubits are merged by a type-I fusion operation, B_{I}, and the coherent-state qubits are mixed by a 50:50 beam splitter, resulting in the state $|H\rangle\,(|\alpha\rangle|i\alpha\rangle + |-\alpha\rangle|-i\alpha\rangle) + |V\rangle\,(|i\alpha\rangle|\alpha\rangle + |-i\alpha\rangle|-\alpha\rangle)$. We count the photon number on one of the CV modes and postselect even photon detection to rule out odd cat states. Then, we have the state $i^n|H\rangle|\mathcal{C}_\alpha^+\rangle + |V\rangle|\mathcal{C}_{i\alpha}^+\rangle$ and the phase i^n can be compensated by a Z gate when $n = 4k + 2$. Note that the DV basis

can be freely interchanged between H/V and $+/-$ using a wave plate. The success probability of $B_{\rm I}$ is 50% and the probability of detecting even photons is approximately 50% when $\alpha \gg 1$. Therefore, we need approximately eight H-coh pairs on average to generate an H-cat pair. Note that any imperfections and loss during the process result in an additional cost of a few more H-cat qubits on average. If we also take into account such additional errors during the generation process of H-cat qubits, the loss thresholds can be slightly degraded, as in Fig. 2(b).

To generate cluster states of hybrid qubits, we employ ancilla qubits, which will be merged by the fusion operation. Here, we choose coherent-state qubits as ancillas and therefore we prepare DV-cat-coherent triples $|\psi_T\rangle = |+\rangle|\mathcal{C}^+_\alpha\rangle|\beta\rangle + |-\rangle|\mathcal{C}^+_{i\alpha}\rangle|-\beta\rangle$ using the scheme shown in Fig. 3(b). The amplitude of the coherent-state qubit β does not need to be the same as the amplitude of the cat-code qubit α but $\beta \gtrsim 1$ is required to suppress the failure probability of the fusion operation. We merge an H-cat pair, $|H\rangle|\mathcal{C}^+_\alpha\rangle + |V\rangle|\mathcal{C}^+_{i\alpha}\rangle$, with an H-coh pair, $|H\rangle|\beta\rangle + |V\rangle|-\beta\rangle$, using $B_{\rm I}$ and obtain the state $|\psi_T\rangle$. In the generation of $|\psi_T\rangle$, we need $2 \times (8+1) = 18$ H-coh pairs on average. In our scheme, we need resource states that are equivalent to cluster states with Hadamard gates applied on some qubits. For that purpose, we prepare a different type of triple state, $|\psi'_T\rangle = |+\rangle|\mathcal{C}^+_\alpha\rangle(|\beta\rangle + |-\beta\rangle) + |-\rangle|\mathcal{C}^+_{i\alpha}\rangle(|\beta\rangle - |-\beta\rangle)$, which can be obtained by rotating the DV basis of a H-coh pair from H/V to $+/-$. Coherent-state qubits are consumed by the fusion operation when generating off-line resource states. The fusion operation is performed by the Bell measurement B_α, which can be implemented using one beam splitter and two PNR detectors [41,131]. It fails if both PNR detectors click on no photon, which occurs with a probability of $p_\alpha = \exp(-2|\beta|^2)$.

In the construction of the RHG lattice, we use two kinds of three-qubit micro H-cluster states, $|C^{\rm c}_3\rangle$ and $|C^{\rm s}_3\rangle$. Typical three-qubit cluster states can be represented as $|C_3\rangle_{123} = \hat{\rm CZ}_{12}\hat{\rm CZ}_{23}|+_1,+_2,+_3\rangle$. The micro cluster states used in our scheme differ by Hadamard gates from typical cluster states. A central micro cluster state is given by $|C^{\rm c}_3\rangle_{102} = \hat{H}_1\hat{H}_2|C_3\rangle_{102} = (|0_1,0_0,0_2\rangle + |1_1,1_0,1_2\rangle)/\sqrt{2}$ and a side micro cluster state is given by $|C^{\rm s}_3\rangle = \hat{H}_1|C_3\rangle_{102} = (|0_1,0_0,0_2\rangle + |1_1,1_0,0_2\rangle + |0_1,0_0,1_2\rangle - |1_1,1_0,1_2\rangle)/2$. The qubit denoted by the subscript 0 in $|C^{\rm c}_3\rangle$ serves as the data qubit or the vertex of the RHG lattice, while the others will be consumed by the hybrid fusion. The generation of $|C^{\rm c}_3\rangle$ is described in Fig. 3(c). We prepare three hybrid triples, $|\psi_T\rangle$, where the second one has two coherent-state qubits that can be obtained by splitting a larger coherent-state qubit with amplitude $\sqrt{2}\beta$. Then, we perform Bell measurements B_α on the coherent-state qubits to merge the three hybrid qubits. We postselect on successful Bell measurements only, so that no error is induced on off-line resource states. The desired state $|C^{\rm c}_3\rangle$ is obtained after applying the appropriate Pauli corrections according to the measurement outcome of B_α. The generation scheme of $|C^{\rm s}_3\rangle$ is almost the same but one needs to replace the last triple state with $|\psi'_T\rangle$. The average number of unit resources to generate a three-qubit cluster state is $54(1-p_\alpha)^{-2}$.

The generation of resource states for gate teleportation, $|\Phi_H\rangle$ and $|\Phi_{\rm CZ}\rangle$, is described in Figs. 3(d) and 3(e), respectively. The Hadamard resource $|\Phi_H\rangle$ can be generated by merging $|\psi_T\rangle$ and $|\psi'_T\rangle$ using B_α. For the CZ resource $|\Phi_{\rm CZ}\rangle$, we need to prepare another type of resource that has two coherent-state ancillas with different bases. To prepare such a state, we merge a triple $|H\rangle|\mathcal{C}^+_\alpha\rangle(|\beta\rangle + |-\beta\rangle) + |V\rangle|\mathcal{C}^+_{i\alpha}\rangle(|\beta\rangle - |-\beta\rangle)$ and an H-coh pair, $|H\rangle|\beta\rangle + |V\rangle|-\beta\rangle$, using $B_{\rm I}$. Once $B_{\rm I}$ is successful, we merge the state with three $|\psi_T\rangle$'s using B_α. The average number of unit resources to generate $|\Phi_H\rangle$ and $|\Phi_{\rm CZ}\rangle$ is, respectively, $36(1-p_\alpha)^{-1}$ and $(18\times 3 + (18+1)\times 2)(1-p_\alpha)^{-3} = 92(1-p_\alpha)^{-3}$.

B. Implementation in other platforms

A DV-CV hybrid entangled pair is employed in our approach as the basic building block of hybrid quantum computation. In the CV part, a bosonic cat-code state needs to be implemented and entangled with a DV qubit such as a single photon. While we focus on all-optical implementation in our analysis, we also emphasize that our hybrid approach is applicable to other platforms. CV qubits in cat states have been successfully demonstrated in superconducting circuits [75–78,103–107], ion traps [62,81,108–114], and circuit acoustic devices [132–134]. In particular, error correction using the cat code has been demonstrated in a superconducting circuit system [76]. Another line of efforts in the superconducting circuit system is a stabilized cat qubit by two-photon driven dissipation [75,77,135,136] or Kerr nonlinear interaction [78,137–141]. By stabilizing the cat-code subspace, a bit-flip error rate is exponentially suppressed, so that it suffices to correct phase-flip error using a simple error-correction code with low overhead [84–86,88,142]. In those schemes, the implementation of a universal gate set preserving the error bias enables hardware-efficient fault-tolerant quantum error correction [84,86,139]. In the presence of CV qubits, any interaction strong enough to entangle the CV qubits with other DV qubits can produce the hybrid qubits. For example, H-cat qubits can be generated by applying a cross-Kerr interaction between DV and CV qubits, acting as $(|+\rangle + |-\rangle)|\mathcal{C}^+_\alpha\rangle \to |+\rangle|\mathcal{C}^+_\alpha\rangle + |-\rangle|\mathcal{C}^+_{i\alpha}\rangle = |+_L\rangle$.

While the required nonlinearity is also within the reach of the current photonic technology [143,144], in other platforms, strong nonlinear interactions between DV and CV qubits are readily available. In trapped-ion systems, a variety of hybrid gate operations have been demonstrated, coupling the internal states of atoms and the phonon modes

[62,108,145,146]. In superconducting circuit QED, universal control of the oscillator mode in a microwave cavity has been demonstrated using nonlinear interaction between the oscillator mode and the transmon qubit [81,109,110,147]. Although those works have restricted the role of the DV mode to the control qubit for manipulating the CV mode, the coupling between the CV mode and a reliable DV qubit will provide us a resource for hybrid quantum computation.

V. DISCUSSION

We have introduced a scheme for fault-tolerant quantum computing based on hybrid qubits combining both CV and DV qubits. We have developed a fault-tolerant architecture in photonic platforms by concatenating CV and DV quantum error-correction codes. A hybrid qubit (H-cat) is defined in the physical level by employing the bosonic cat code in the CV part and a single photon in the DV part. The effect of photon loss is readily correctable via the cat code in each H-cat qubit and the error caused by nonorthogonality is removed. We have proposed two types of hybrid-fusion schemes as the building blocks for both circuit-based and measurement-based quantum computing, to design fault-tolerant architecture based on an outer DV quantum error-correction code such as the Steane [98] and surface codes [99–101], implemented in the RHG lattice. We have shown that the proposed hybrid approach allows us to achieve 4-times-higher loss thresholds than existing CV and hybrid approaches and is at least an order of magnitude more resource efficient compared to previous proposals in photonic platforms.

Bosonic encoding with coherent or cat states in CV qubits generally exhibits a trade-off between the X error and Z error rates, which are induced predominantly from the ambiguity of the logical basis and photon loss, respectively. Note that any cat states are more fragile to photon loss, i.e., the Z error rate increases as the amplitude α gets larger, while the bases become more distinguishable to each other, i.e., the X error rate decreases [41,50,102,124]. In this circumstance, the proposed hybrid scheme aims to reduce the X error rate significantly by increasing the amplitude α while suppressing the increase of the Z error rate by means of the bosonic cat-code encoding on the physical level. This is how our scheme achieves the record-high loss thresholds among the schemes using cat-state encoding or their hybrid. Moreover, although the H-cat qubit is 8 times as expensive as the H-coh qubit in photonic platforms, as estimated in Sec. IV A, we have demonstrated that employing the bosonic cat code in the physical level (the H-cat) can also improve the resource efficiency by about a factor of 13 compared to only coherent- or cat-state encoding (the H-coh) in hybrid quantum computing. The resource efficiency of our scheme is due to the fact that H-cat qubits inherit the benefit of bosonic CV quantum error correction. In this sense, a comparison of our scheme with the MBQC with the cat code only is to be expected in further work; this has not been rigorously studied so far and is currently being investigated in the photonic platform [148].

In our analysis of the thresholds, the error model in the physical level has been estimated mainly based on the effect of photon loss, which is the predominant source of error in the photonic platform. We note that other types of errors, such as phase shifting, are hardly caused by hybrid-fusion operations, i.e., in beam splitters and photon-number-counting detectors. On the other hand, the phase error that may occur in logical gate operations is detrimental and should be suppressed. A set of bias-preserving gate operations can be considered to prevent further propagation of errors to other hybrid qubits [84,86,139]. A controlled rotation can be also employed to suppress phase error if sufficient nonlinear interaction is available, as illustrated in Ref. [91]. Further, in the fault-tolerance architecture, any errors in the logical level caused as a result of physical-level or universal gate operations are handled by outer quantum error-correction codes, e.g., in our simulation, the surface code in the RHG lattice.

To realize full fault-tolerant quantum computing with H-cat qubits, encoding with amplitude $\alpha \gtrsim 2$ in the CV part is required, while its maximum performance is achieved with $\alpha \approx 2.93$, as presented in Fig. 2(b). Despite still being challenging in photonic platforms, there has been a lot of progress in generating cat states with large amplitude both experimentally [97,149,150] and theoretically [151–154]. The PNR detector is another requirement in the realization of our scheme. The maximum performance of our scheme requires the resolution $\bar{n} = \alpha^2 \approx 8.58$, which is within the reach of currently available detectors with a resolution of up to 16 photons and 98% efficiency [155]. We thus expect that our hybrid scheme will be available with current and near-term devices.

While we have discussed mainly hybrid quantum computation in all-photonic platforms, we emphasize again that our scheme is generally applicable to other hybrid platforms including superconducting and trapped-ion systems, details of which are discussed in Sec. IV B. Furthermore, it may be valuable to extend our scheme to combine with the fault-tolerant architecture concatenated with the bosonic cat code in superconducting systems [86]. Considering the biased errors under loss in cat-state encoding in the CV part, other DV quantum error-correction codes may be also useful for concatenation in architecture, such as repetition [84,86,142] and $XZZX$ [156–158] codes to enhance the loss thresholds, as well as the resource efficiency, further. Another interesting method to pursue is to explore hybrid encoding using squeezed-cat qubits [107,159–161], which has favorable error-bias properties with a reduced excitation number and the partial correction of excitation loss

errors. As the thresholds have been widely investigated for stabilized cat qubits [86,88,142,157] and for GKP qubits [89,90,92,96] in superconducting systems, a hybrid approach incorporating DV qubits would be expected to improve their performance. For hybridization between the CV and DV qubits, nonlinear interactions, which are readily available in superconducting or trapped-ion systems [62,81,108–110,145–147], can play an important role. A hybrid architecture compromising GKP qubits and squeezed vacuum states can be also considered in the photonic platform [94].

The hybrid approach using CV-DV hybrid qubits is also generally useful and can be extended further for other quantum information-processing tasks, e.g., quantum communications or sensing, which we leave as future work. We believe that our approach opens up a novel way to bring about a synergy between CV and DV hybrid platforms toward scalable fault-tolerant quantum computing.

ACKNOWLEDGMENTS

This research was funded by the Korea Institute of Science and Technology (Grant No. 2E32941) and the National Research Foundation of Korea (Grant No. 2022M3K4A1094774). S.H.L. and H.J. are supported by National Research Foundation of Korea (NRF) grants funded by the Korean government (Grants No. 2023R1A2C1006115 and No. 2022M3K4A1097117) and by an Institute of Information & Communications Technology Planning & Evaluation (IITP) grant funded by the Korean government (MSIT) (Grants No. IITP-2021-0-01059 and No. IITP-2023-2020-0-01606). S.H.L. is supported by the Australian Research Council via the Centre of Excellence in Engineered Quantum Systems (EQUS) project number CE170100009. L.J. acknowledges support from the Army Research Office (ARO) (Grant No. W911NF-23-1-0077), ARO Multidisciplinary University Initiative (MURI) (Grant No. W911NF-21-1-0325), Air Force Office of Scientific Research (AFOSR) MURI (Grants No. FA9550-19-1-0399, No. FA9550-21-1-0209, and No. FA9550-23-1-0338), the National Science Foundation (NSF) (Grants No. OMA-1936118, No. ERC-1941583, No. OMA-2137642, No. OSI-2326767, and No. CCF-2312755), NTT Research, and the Packard Foundation (Grant No. 2020-71479).

APPENDIX A: HYBRID FUSION

The hybrid-fusion operation is a key ingredient of our hybrid quantum computation, which also implements photon-loss correction. In this appendix, we present the details of hybrid fusion. The fusion is composed of two Bell measurements, one for DV qubits and the other for cat-code qubits.

1. Hybrid-fusion operation

The hybrid-fusion operation can be done by performing Bell measurement on CV qubits and DV qubits, i.e., $B_{\mathcal{C}}$ and $B_{\mathcal{D}}$, respectively. Hybrid Bell states can be represented, in the basis of Bell states of CV and DV qubits, as

$$\begin{aligned}|\Psi_L^{\pm}\rangle &= \frac{1}{\sqrt{2}}\left(|+,\mathcal{C}_\alpha^+\rangle|-,\mathcal{C}_{i\alpha}^+\rangle \pm |-,\mathcal{C}_{i\alpha}^+\rangle|+,\mathcal{C}_\alpha^+\rangle\right)\\ &= \frac{1}{2}\left[\left(|\Phi_{\mathcal{D}}^-\rangle + |\Psi_{\mathcal{D}}^-\rangle\right)\left(\frac{|\Psi_{\mathcal{C}}^+\rangle}{2\mathcal{N}_C^{B+}} + \frac{|\Psi_{\mathcal{C}}^-\rangle}{2\mathcal{N}_C^{B-}}\right)\right.\\ &\qquad \left.\pm\left(|\Phi_{\mathcal{D}}^-\rangle - |\Psi_{\mathcal{D}}^-\rangle\right)\left(\frac{|\Psi_{\mathcal{C}}^+\rangle}{2\mathcal{N}_C^{B+}} - \frac{|\Psi_{\mathcal{C}}^-\rangle}{2\mathcal{N}_C^{B-}}\right)\right]\\ &= \frac{1}{2}\left(|\Phi_{\mathcal{D}}^-\rangle|\tilde{\Psi}_{\mathcal{C}}^{\pm}\rangle + |\Psi_{\mathcal{D}}^-\rangle|\tilde{\Psi}_{\mathcal{C}}^{\mp}\rangle\right) \qquad \text{(A1)}\end{aligned}$$

and, similarly,

$$|\Phi_L^{\pm}\rangle = \frac{1}{2}\left(|\Phi_{\mathcal{D}}^+\rangle|\tilde{\Phi}_{\mathcal{C}}^{\pm}\rangle + |\Psi_{\mathcal{D}}^+\rangle|\tilde{\Phi}_{\mathcal{C}}^{\mp}\rangle\right). \qquad \text{(A2)}$$

Let us first consider that the CV Bell state is determined without ambiguity. Then, the letter of the hybrid Bell state is determined in the same way as that of the CV part. To determine the sign, we only need the letter information of the DV Bell state, i.e., the sign of the CV part and the hybrid is the same (flipped) if the letter of the DV part is Φ (Ψ). Even though the DV Bell measurement $B_{\mathcal{D}}$ fails, the letter of the DV part is perfectly distinguished and therefore we can always determine the hybrid Bell state without ambiguity.

If there is a letter ambiguity in the CV Bell measurement, the ambiguity is removed if we have the sign information of the DV part, i.e., $B_{\mathcal{D}}$ succeeds. The ambiguity only remains when $B_{\mathcal{C}}$ has an ambiguity and $B_{\mathcal{D}}$ fails and it causes an X error with the rate $P_X = \frac{1}{2}p_X$. We summarize the outcome decision of hybrid fusion in Fig. 4(d).

2. Fusion in the CV part

The cat code is designed to protect qubits against photon loss [68,69], which is the predominant type of error in optical systems. The key idea of the four-component cat code is that we encode qubits in the subspace of even-photon-number states and an error is detected when the parity changes. Specifically, the code space is defined by even cat states $\left\{|\mathcal{C}_\alpha^+\rangle, |\mathcal{C}_{i\alpha}^+\rangle\right\}$, where $|\mathcal{C}_\alpha^+\rangle = \mathcal{N}_{\mathcal{C}}^+(|\alpha\rangle + |-\alpha\rangle)$, with the normalization factor $\mathcal{N}_{\mathcal{C}}^+ \equiv 1/\sqrt{2(1+e^{-2\alpha^2})}$, and $|\alpha\rangle$ is a coherent state with amplitude α. A photon loss can be modeled by application of the annihilation operator, so that the state evolves into the odd cat states as $\hat{a}|\mathcal{C}_\alpha^+\rangle \propto |\mathcal{C}_\alpha^-\rangle = \mathcal{N}_{\mathcal{C}}^-(|\alpha\rangle - |-\alpha\rangle)$, where $\mathcal{N}_{\mathcal{C}}^- \equiv 1/\sqrt{2(1-e^{-2\alpha^2})}$ is the normalization factor. Further, photon loss induces a phase

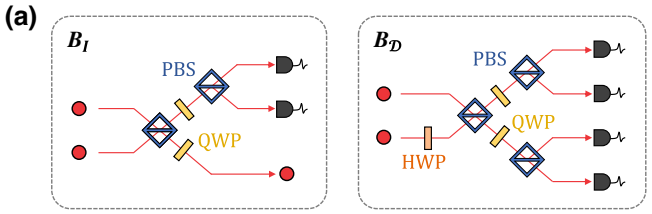

(d)

B_C	B_D	Decision	X error
Perfect	Success	Sign flipped from CV	None
	Fail	The same as CV	None
Letter ambiguous	Success	Sign flipped from CV	None
	Fail	The same as CV	$P_X = \frac{1}{2}p_X$

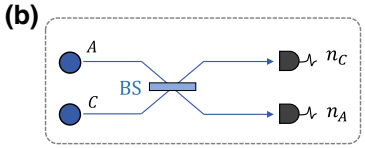

Measurement Pattern	No photon loss			Single photon loss		
	N	Decision	X error	N	Decision	X error
$n_A = 0$ or $n_C = 0$	$4k$	$\lvert\Phi_C^+\rangle$	p_X	$4k+3$	$\lvert\Phi_C^+\rangle$	p_X
	$4k+2$	$\lvert\Phi_C^-\rangle$	None	$4k+1$	$\lvert\Phi_C^-\rangle$	None
$n_A \neq 0$ and $n_C \neq 0$	$4k$	$\lvert\Psi_C^+\rangle$		$4k+3$	$\lvert\Psi_C^+\rangle$	
	$4k+2$	$\lvert\Psi_C^-\rangle$		$4k+1$	$\lvert\Psi_C^-\rangle$	

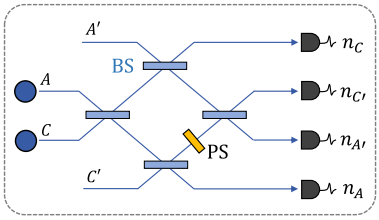

Measurement pattern	No photon loss			Single photon loss		
	N	Decision	X error	N	Decision	X error
$[0, n_C, n_{A'}, n_{C'}]$ $[n_A, 0, n_{A'}, n_{C'}]$ $[0,0, n_{A'}, n_{C'}]$	$4k$	$\lvert\Phi_C^+\rangle$	None	$4k+3$	$\lvert\Phi_C^+\rangle$	None
	$4k+2$	$\lvert\Phi_C^-\rangle$		$4k+1$	$\lvert\Phi_C^-\rangle$	
$[n_A, n_C, 0, n_{C'}]$ $[n_A, n_C, n_{A'}, 0]$ $[n_A, n_C, 0,0]$	$4k$	$\lvert\Psi_C^+\rangle$		$4k+3$	$\lvert\Psi_C^+\rangle$	
	$4k+2$	$\lvert\Psi_C^-\rangle$		$4k+1$	$\lvert\Psi_C^-\rangle$	
Others	$4k$	$\lvert\Psi_C^+\rangle$ or $\lvert\Phi_C^+\rangle^*$	p_X	$4k+3$	$\lvert\Psi_C^+\rangle$ or $\lvert\Phi_C^+\rangle^*$	p_X
	$4k+2$	$\lvert\Psi_C^-\rangle$ or $\lvert\Phi_C^-\rangle^*$		$4k+1$	$\lvert\Psi_C^-\rangle$ or $\lvert\Phi_C^-\rangle^*$	

FIG. 4. (a) Schemes of type-I fusion operation B_I and type-II fusion operation B_D: PBS, polarizing beam splitter; QWP, quarter-wave plate; HWP, half-wave plate. On-off detectors suffice for Bell measurements in ideal cases, while detectors are required to resolve up to two photons in order to distinguish photon-loss cases. (b) The scheme for the Bell measurement of cat-code qubits using one beam splitter (BS) and two PNR detectors [115]. The measurement outcome is determined by following the table. (c) The scheme for the Bell measurement of cat-code qubits using four BSs, one $\pi/2$ phase shifter (PS), and four PNR detectors [116]. Two ancilla modes, A' and C', are prepared in vacuum. The decision of the measurement outcome is summarized in the table. We explicitly indicate n_j, where $j \in \{A, C, A', C'\}$, other than 0 if the detector clicks on at least one photon. (d) The outcome decision of the hybrid-fusion operation. The decision is made by collecting the information of B_C and B_D.

shift on $|\mathcal{C}_{i\alpha}^+\rangle$, i.e., $\hat{a}|\mathcal{C}_{i\alpha}^+\rangle \propto i|\mathcal{C}_{i\alpha}^-\rangle$, which may cause a Z error unless the parity change is detected by the measurement. Thus a parity measurement can play the role of syndrome measurement to detect a photon-loss event. Such a measurement has been demonstrated in the superconducting circuit system via nonlinear interaction with an ancilla transmon qubit [76].

In optical systems, two separate works have recently proposed schemes for Bell measurement of the four-component cat code [115,116], which also detects single-photon loss. The cat-code Bell measurement distinguishes four Bell states, $|\Psi_C^\pm\rangle = \mathcal{N}_C^{B\pm}(|\mathcal{C}_\alpha^+\rangle|\mathcal{C}_{i\alpha}^+\rangle \pm |\mathcal{C}_{i\alpha}^+\rangle|\mathcal{C}_\alpha^+\rangle)$ and $|\Phi_C^\pm\rangle = \mathcal{N}_C^{B\pm}(|\mathcal{C}_\alpha^+\rangle|\mathcal{C}_\alpha^+\rangle \pm |\mathcal{C}_{i\alpha}^+\rangle|\mathcal{C}_{i\alpha}^+\rangle)$, with the normalization factor $\mathcal{N}_C^{B\pm} = \cosh\alpha^2/\sqrt{2(\cosh^2\alpha^2 \pm \cos^2\alpha^2)}$. The schemes only use linear optical elements and PNR detectors, as depicted in Figs. 4(b) and 4(c). Measurement patterns on PNR detectors differ by the parity of the input ports. In what follows, we will use the notation {even(odd), even(odd)} to represent the photon-number parity of input modes A and C and define N to be the total number of photons detected.

a. Scheme of Hastrup and Andersen [115]

The scheme proposed by Hastrup and Andersen (HA) is composed of one beam splitter and two PNR detectors, as depicted in Fig. 4(b). The transformation of coherent states by a beam splitter is described as

$$|\alpha_A\rangle_A|\alpha_C\rangle_C \to \left|\frac{\alpha_A+\alpha_C}{\sqrt{2}}\right\rangle_A \left|\frac{\alpha_A-\alpha_C}{\sqrt{2}}\right\rangle_C. \tag{A3}$$

The PNR detectors count the photon numbers of modes A and C, which we denote by n_A and n_C, respectively. If the input state is a superposition of $|\mathcal{C}_\alpha^+\rangle|\mathcal{C}_\alpha^+\rangle$ and $|\mathcal{C}_{i\alpha}^+\rangle|\mathcal{C}_{i\alpha}^+\rangle$, where every term in the coherent-state basis is given by either $\alpha_A = \alpha_C$ or $\alpha_A = -\alpha_C$, at least one of the detectors must click on no photon. In other words, if $n_A = 0$ or $n_C = 0$, we guess that the letter of the input Bell state is Φ and, otherwise, we guess that the letter is Ψ. On the other hand, the sign can be distinguished by the total number of photon detected, N. In the ideal case without photon loss, where the input parity is {even, even}, a simple calculation yields that the sign is determined as $+$ for $N = 4k$ and $-$ for $N = 4k + 2$, where k is a nonnegative integer.

Let us consider the case in which a single photon is lost from one of the modes A or C, where the input parity becomes {odd, even} or {even,odd}. The photon loss only changes the relative phase between superposed coherent states but does not change the amplitude of coherent states in phase space. Therefore, we can apply the same letter-decision strategy. Due to the single-photon loss, the sign is determined as $+$ for $N = 4k + 3$ and $-$ for $N = 4k + 1$. The outcome decision is summarized in the table of Fig. 4(b), for the photon-loss case as well as for the ideal case.

If a single photon is lost from each input port so that the input parity is {odd, odd}, we follow the outcome decision of the ideal case because N is even. A Z error is induced by a phase shift on $|\mathcal{C}_{i\alpha}^+\rangle$ and it can be corrected only if the measurement pattern distinguishes whether the input parity is {even, even} or {odd, odd}. In the case in which both n_A and n_C are nonzero, a straightforward calculation yields that $n_C = n_A \pmod 4$ for {even, even} input and $n_C = n_A + 2 \pmod 4$ for {odd, odd} input and thus the Z error is correctable. Otherwise, the Z error remains undetected, the probability of which is given by

$$p_{Z|\mathrm{OO}}(\alpha) = \frac{1}{2} + \frac{1}{2}\,\mathrm{csch}^2\,\alpha^2(\cosh\alpha^2 - \cos\alpha^2), \tag{A4}$$

where the subscript OO represents the fact that the Z error occurs for {odd, odd} input.

There exists a small probability of misidentifying Ψ as Φ because a no-photon click can occur for a coherent state with nonzero amplitude. Once we obtain the measurement pattern with $n_A = 0$ or $n_C = 0$, we have an ambiguity in the letter, which causes an X error. We can locate such an X error and denote by p_{loc} and p_X, respectively, the probability of locating the X error and the total X error rate. In general, the probability depends on the input state but in our hybrid quantum computation, it suffices to calculate the probability for the basis states $|\mathcal{C}_\alpha^\pm\rangle$ and $|\mathcal{C}_{i\alpha}^\pm\rangle$, because they are accompanied by orthogonal DV qubit states $|+\rangle$ and $|-\rangle$, respectively. Even though the DV qubit is lost, the CV qubit remains in a mixture of $|\mathcal{C}_\alpha^\pm\rangle$ and $|\mathcal{C}_{i\alpha}^\pm\rangle$ due to dephasing. We assume that the input state is equally distributed among $|\mathcal{C}_\alpha^\pm\rangle|\mathcal{C}_\alpha^\pm\rangle$, $|\mathcal{C}_\alpha^\pm\rangle|\mathcal{C}_{i\alpha}^\pm\rangle$, $|\mathcal{C}_{i\alpha}^\pm\rangle|\mathcal{C}_\alpha^\pm\rangle$, and $|\mathcal{C}_{i\alpha}^\pm\rangle|\mathcal{C}_{i\alpha}^\pm\rangle$. A direct calculation yields that the locatable error probability is given by

$$\begin{aligned}
p_{\mathrm{loc}|\mathrm{EE}}(\alpha) &= \frac{1}{2} + \frac{1}{2}\,\mathrm{sech}^2\,\alpha^2(\cosh\alpha^2 + \cos\alpha^2 - 1),\\
p_{\mathrm{loc}|\mathrm{EO}}(\alpha) &= \frac{1}{2} + \frac{1}{2}\,\mathrm{sech}\,\alpha^2,\\
p_{\mathrm{loc}|\mathrm{OO}}(\alpha) &= \frac{1}{2} + \frac{1}{2}\,\mathrm{csch}^2\,\alpha^2(\cosh\alpha^2 - \cos\alpha^2),
\end{aligned} \tag{A5}$$

where the subscripts EE, EO, and OO denote, respectively, the input parities {even, even}, {even, odd}, and {odd, odd}. Further, the total X error rate is written as

$$\begin{aligned}
p_{X|\mathrm{EE}}(\alpha) &= \frac{1}{2}\,\mathrm{sech}^2\,\alpha^2(\cosh\alpha^2 + \cos\alpha^2 - 1),\\
p_{X|\mathrm{EO}}(\alpha) &= \frac{1}{2}\,\mathrm{sech}\,\alpha^2,\\
p_{X|\mathrm{OO}}(\alpha) &= \frac{1}{2}\,\mathrm{csch}^2\,\alpha^2(\cosh\alpha^2 - \cos\alpha^2).
\end{aligned} \tag{A6}$$

It is straightforward to observe that $p_{\mathrm{loc}} = \frac{1}{2} + p_X$ for any input parity, where the term $\frac{1}{2}$ represents the fact that input states $|\mathcal{C}_\alpha^\pm\rangle|\mathcal{C}_\alpha^\pm\rangle$ and $|\mathcal{C}_{i\alpha}^\pm\rangle|\mathcal{C}_{i\alpha}^\pm\rangle$ always fall into unambiguous measurement patterns and the latter term represents the probability of misidentifying Ψ as Φ.

b. Scheme of Su *et al.* [116]

The scheme proposed by Su, Dhand, and Ralph (SDR) is composed of two ancilla modes prepared in vacuum, four beam splitters, one phase shifter, and four PNR detectors, as depicted in Fig. 4(c). The transformation of coherent states by linear optical elements is described as

$$|\alpha_A\rangle_A|\alpha_C\rangle_C|\mathrm{vac}\rangle_{A'}|\mathrm{vac}\rangle_{C'} \to \left|\frac{\alpha_A + \alpha_C}{2}\right\rangle_A\left|\frac{\alpha_A - \alpha_C}{2}\right\rangle_C\left|\frac{-1+i}{2\sqrt{2}}\alpha_A + \frac{1+i}{2\sqrt{2}}\alpha_C\right\rangle_{A'}\left|\frac{1+i}{2\sqrt{2}}\alpha_A + \frac{-1+i}{2\sqrt{2}}\alpha_C\right\rangle_{C'}, \tag{A7}$$

where $|\mathrm{vac}\rangle$ represents a vacuum state. The PNR detectors count the photon numbers of modes A, C, A', and C', which we denote by n_A, n_C, $n_{A'}$, and $n_{C'}$, respectively. In the basis of the four-headed cat code, at least one of the detectors must click on no-photon, such that

$$\begin{cases} n_A = 0, & \text{if } \alpha_C = -\alpha_A, \\ n_C = 0, & \text{if } \alpha_C = \alpha_A, \\ n_{A'} = 0, & \text{if } \alpha_C = -i\alpha_A, \\ n_{C'} = 0, & \text{if } \alpha_C = i\alpha_A. \end{cases} \tag{A8}$$

Thus, if we obtain a measurement pattern with $n_{A'} = 0$ or $n_{C'} = 0$, we guess that the input state is a superposition of $|\mathcal{C}_\alpha^+\rangle|\mathcal{C}_{i\alpha}^+\rangle$ and $|\mathcal{C}_\alpha^+\rangle|\mathcal{C}_{i\alpha}^+\rangle$, i.e., the letter of the Bell state is Ψ. Similarly, if $n_A = 0$ or $n_C = 0$, we guess that the letter of the input Bell state is Φ. The sign is determined as $+$ for $N = 4k$ and $-$ for $N = 4k + 2$ in the ideal case. In the case of single-photon loss, the letter is determined in the same way and the sign is determined as $+$ for $N = 4k + 3$ and $-$ for $N = 4k + 1$. The decision of the measurement outcome is summarized in the table of Fig. 4(c).

The Z error induced from an $\{\text{odd}, \text{odd}\}$ input is correctable by a few measurement patterns. For the measurement pattern with $n_A > 0$, $n_C > 0$, and $n_{A'} = n_{C'} = 0$, n_A and n_C are related by $n_A = n_C \pmod 4$ for $\{\text{even}, \text{even}\}$ input, while $n_A = n_C + 2 \pmod 4$ for $\{\text{odd}, \text{odd}\}$ input. For the measurement pattern with $n_A = n_C = 0$, $n_{A'} > 0$, and $n_{C'} > 0$, we can distinguish the input parity in a similar way.

We can distinguish one of four Bell states with certainty if the no-photon click occurs only on one side of detectors $\{A, C\}$ or $\{A', C'\}$. However, in some cases, a no-photon click may occur on both sides of the detectors, because there is chance of a no-photon click on other modes in coherent states with nonzero amplitude. In such cases, we have an ambiguity on the letter of the Bell state. For example, for the measurement pattern with $n_A = n_{A'} = 0$, $n_C > 0$, and $n_{C'} > 0$, the projected state is $2^{-n_C/2}|\Psi_{\mathcal{C}}^{\pm}\rangle + 2^{-n_{C'}/2}|\Phi_{\mathcal{C}}^{\pm}\rangle$. If $n_{C'} > n_C$, we take the state with higher probability $|\Psi_{\mathcal{C}}^{\pm}\rangle$, assigning an X error rate $p_X = 2^{-n_{C'}}/(2^{-n_C} + 2^{-n_{C'}})$ and vice versa. If $n_C = n_{C'}$, we randomly choose one of two states $|\Psi_{\mathcal{C}}^{\pm}\rangle$ or $|\Phi_{\mathcal{C}}^{\pm}\rangle$, assigning an X error rate $p_X = \frac{1}{2}$. The same strategy is applied for the other measurement patterns as well.

The probability of an uncorrectable Z error is given by

$$p_{Z|\mathrm{OO}}(\alpha) = \operatorname{csch}^2\alpha^2 \left(\tfrac{1}{2}\cosh(2\alpha^2) - \cosh\alpha^2 + 2\cosh\tfrac{\alpha^2}{2} - 2\cos\tfrac{\alpha^2}{2} + \tfrac{1}{2}\right). \tag{A9}$$

The probability of obtaining measurement patterns with an X error is written as

$$\begin{aligned} p_{\mathrm{loc}|\mathrm{EE}}(\alpha) &= \operatorname{sech}^2\alpha^2 \left(\cosh\tfrac{3\alpha^2}{2} - \tfrac{1}{2}\cosh\alpha^2 + \cos\tfrac{\alpha^2}{2} - \tfrac{1}{2}\right), \\ p_{\mathrm{loc}|\mathrm{EO}}(\alpha) &= \operatorname{sech}\frac{\alpha^2}{2} + \frac{1}{2}\operatorname{sech}\alpha^2 \left(\operatorname{sech}^2\frac{\alpha^2}{2} - 1\right), \\ p_{\mathrm{loc}|\mathrm{OO}}(\alpha) &= \operatorname{csch}^2\alpha^2 \left(\cosh\tfrac{3\alpha^2}{2} - \tfrac{1}{2}\cosh\alpha^2 - \cos\tfrac{\alpha^2}{2} + \tfrac{1}{2}\right). \end{aligned} \tag{A10}$$

Since the explicit calculation of the total X error rate p_X is not straightforward, we perform a numerical calculation instead.

In Fig. 5, we plot the locatable error rate p_{loc} and the X error rate p_X for both the HA scheme and the SDR scheme. The error rates are slightly different for different input parities but they almost overlap, especially when $\alpha > 2$. It is shown that the total X error rate exponentially decreases for both schemes, while the HA scheme exhibits much a lower error rate. On the other hand, the probability of locating the error is much lower for the SDR scheme, while it is almost constant for the HA scheme even for large α. That is because the measurement patterns to detect Φ always have an ambiguity of misidentifying Ψ even though the actual error rate is very small. Therefore, the SDR scheme is beneficial in the case in which we need an unambiguous discrimination of the Bell state without error, while the HA scheme works better when we need to suppress the actual error rate without postselection.

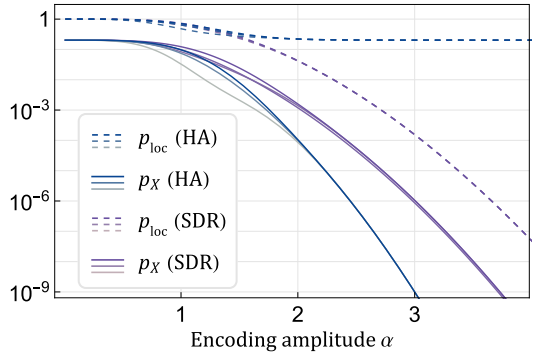

FIG. 5. The error rates in the Bell measurement of cat-code qubits using the HA scheme (blue) and the SDR scheme (purple). The solid curves represent the total X error rate and the dashed curves represent the probability of locating the X error. Each curve is an overlap of three curves representing different input parities, while they are almost the same for large α.

3. Fusion in the DV part

For the polarization qubit, we employ two types of Bell measurements, called the type-I fusion operation and the type-II fusion operation [14], depicted in Fig. 4(a). The type-I fusion operation $B_{\rm I}$ performs a partial Bell measurement that outputs one qubit from a two-qubit input. If only one is detected, the operation is described as $|+\rangle\langle H|\langle H| - |-\rangle\langle V|\langle V|$ for an H click or as $|H\rangle\langle H|\langle H| + |V\rangle\langle V|\langle V|$ for a V click. If two photons or no photons are detected, the measurement fails, which occurs with probability $1/2$. This operation plays a role of connecting qubits in two separate cluster states. In the resource generation described in Sec. IV A, $B_{\rm I}$ is employed to merge hybrid entangled states.

The type-II fusion operation $B_{\rm II}$, or $B_{\mathcal{D}}$ in this paper, performs an incomplete Bell measurement that distinguishes only two of four Bell states. If one detector from the upper two and another from the lower two click at the same time, the measurement succeeds, yielding the results $|\Psi_{\mathcal{D}}^{+}\rangle = \frac{1}{\sqrt{2}}(|H\rangle|V\rangle + |V\rangle|H\rangle)$ for (H,V) or (V,H) clicks and $|\Psi_{\mathcal{D}}^{-}\rangle = \frac{1}{\sqrt{2}}(|H\rangle|V\rangle - |V\rangle|H\rangle)$ for (H,H) or (V,V) clicks. If two photons are detected simultaneously at upper or lower detectors, the measurement fails, but we can obtain the information that the state is one of two Bell states $|\Phi_{\mathcal{D}}^{\pm}\rangle = \frac{1}{\sqrt{2}}(|H\rangle|H\rangle \pm |V\rangle|V\rangle)$, i.e., the sign is Φ. In an ideal case, the failure occurs with probability $1/2$. If any of the DV photons are lost, $B_{\mathcal{D}}$ can only detect one photon or no photons and the information on the input DV Bell state is completely lost. To distinguish between the photon loss and the failure, detectors are required to resolve up to two photons.

APPENDIX B: GATE OPERATIONS OF HYBRID QUBITS

In this appendix, we present gate operations of hybrid qubits, required for universal quantum computation. In order to perform universal quantum computation, we choose the gate set $\{\hat{X}, \hat{Z}_\theta, \hat{H}, \hat{\rm CZ}\}$. $\hat{X}$ and $\hat{Z}_\theta$ can be implemented only using linear optical elements, as depicted in Fig. 6(a). The Pauli-X can be implemented by applying bit-flip operations on both CV and DV qubits, using a polarization rotator acting as $|+\rangle \leftrightarrow |-\rangle$ and a $\pi/2$ phase shifter acting as $|\mathcal{C}_\alpha^{+}\rangle \leftrightarrow |\mathcal{C}_{i\alpha}^{+}\rangle$. The arbitrary rotation along the Z axis, $\hat{Z}_\theta$, can be done by applying the θ phase shift only on the DV qubit as $|+\rangle \to |+\rangle, |-\rangle \to e^{i\theta}|-\rangle$, implemented by a half-wave plate sandwiched by two quarter-wave plates. To perform Hadamard ($\hat{H}$) and controlled-Z ($\hat{\rm CZ}$) gates, we employ the gate-teleportation technique.

The essential ingredients for the teleportation are an entangled state and the Bell measurement, as depicted in Fig. 6(b). The hybrid Bell measurement is done by the fusion operation that we have described in Appendix A. We accomplish the teleportation by applying appropriate

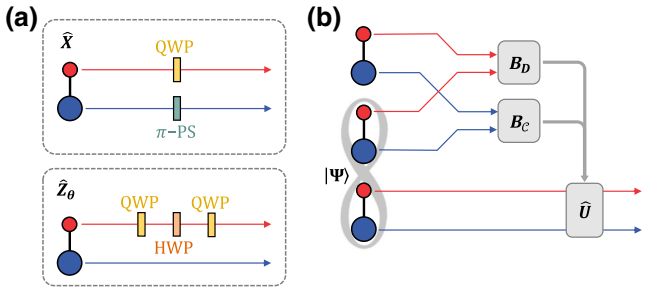

FIG. 6. (a) The optical implementation of single-qubit-rotation gates. $\hat{X}$ can be implemented using a half-wave plate (HWP) on the DV qubit and a π phase shifter (PS) on the CV qubit. $\hat{Z}_\theta$ can be implemented using an HWP sandwiched by two quarter-wave plates (QWPs), where the rotation angle θ is adjusted by rotating the HWP. (b) The schematics for the teleportation of hybrid qubits. The measurement outcome of hybrid fusion is sent via the classical channel and is used for Pauli correction.

Pauli correction according to the measurement outcome of the hybrid fusion. In fact, we do not need to physically perform Pauli operations; they can be done by updating the Pauli frame [15]. The gate teleportation can be done by employing an appropriate entangled channel. For instance, the Hadamard gate $\hat{H}$ can be performed using the resource state $|\Phi_H\rangle \propto |0_L,0_L\rangle + |0_L,1_L\rangle + |1_L,0_L\rangle - |1_L,1_L\rangle$ and the $\hat{\rm CZ}$ gate can be performed with two teleportation circuits using $|\Phi_{\rm CZ}\rangle \propto |0_L,0_L,0_L,0_L\rangle + |0_L,0_L,1_L,1_L\rangle + |1_L,1_L,0_L,0_L\rangle - |1_L,1_L,1_L,1_L\rangle$. The generation scheme of the resource states is presented in Sec. IV A.

The measurement in the Z basis can be performed by the measurement on the DV qubit using a polarization measurement. The phase measurement on the CV qubit may also accomplish the Z-basis measurement but requires nonlinear operations [91]. The heterodyne measurement can be a candidate for the cat-code measurement, taking practical advantages at the cost of a high probability of misreading.

APPENDIX C: ERROR MODEL

1. State evolution under lossy channel

Photon losses are major obstacles in optical quantum computing. The interaction with the lossy environment is described by the master equation [162]

$$\frac{d\rho}{dt} = \gamma \sum_j \left(\hat{a}_j \rho \hat{a}_j^\dagger - \frac{1}{2}\hat{a}_j^\dagger \hat{a}_j \rho - \frac{1}{2}\rho \hat{a}_j^\dagger \hat{a}_j \right), \tag{C1}$$

where j runs over the DV and CV modes and the loss rate is given by $\eta = 1 - \exp(-\gamma t)$. We introduce the formula for the evolution in the coherent-state basis, written as [162]

$$|\alpha\rangle\langle\beta| \to \langle\beta|\alpha\rangle^\eta |\sqrt{1-\eta}\alpha\rangle\langle\sqrt{1-\eta}\beta|. \tag{C2}$$

With this formula, a straightforward calculation leads to the expression for the evolution of an arbitrary hybrid qubit, $|\psi\rangle = a|+\rangle|\mathcal{C}^+_\alpha\rangle + b|+\rangle|\mathcal{C}^+_{i\alpha}\rangle$, written as

$$\rho = (1-\eta)\sum_{l=0}^{3} A_l |\psi'_{(l)}\rangle\langle\psi'_{(l)}| + \eta\left(B_0\tau_{(0)} + B_1\tau_{(1)}\right), \tag{C3}$$

where

$$\begin{aligned}
|\psi'_{(0)}\rangle &= a|+\rangle|\mathcal{C}^+_{\alpha'}\rangle + b|-\rangle|\mathcal{C}^+_{i\alpha'}\rangle,\\
|\psi'_{(1)}\rangle &= a|+\rangle|\mathcal{C}^-_{\alpha'}\rangle + ib|-\rangle|\mathcal{C}^-_{i\alpha'}\rangle,\\
|\psi'_{(2)}\rangle &= a|+\rangle|\mathcal{C}^+_{\alpha'}\rangle - b|-\rangle|\mathcal{C}^+_{i\alpha'}\rangle,\\
|\psi'_{(3)}\rangle &= a|+\rangle|\mathcal{C}^-_{\alpha'}\rangle - ib|-\rangle|\mathcal{C}^-_{i\alpha'}\rangle,\\
\tau_{(0)} &= |\mathrm{vac}\rangle\langle\mathrm{vac}| \otimes \left(|a|^2|\mathcal{C}^+_{\alpha'}\rangle\langle\mathcal{C}^+_{\alpha'}| + |b|^2|\mathcal{C}^+_{i\alpha'}\rangle\langle\mathcal{C}^+_{i\alpha'}|\right),\\
\tau_{(1)} &= |\mathrm{vac}\rangle\langle\mathrm{vac}| \otimes \left(|a|^2|\mathcal{C}^-_{\alpha'}\rangle\langle\mathcal{C}^-_{\alpha'}| + |b|^2|\mathcal{C}^-_{i\alpha'}\rangle\langle\mathcal{C}^-_{i\alpha'}|\right).
\end{aligned} \tag{C4}$$

Note that the amplitude of the coherent states is reduced to $\alpha' = \sqrt{1-\eta}\alpha$. The coefficients are explicitly given by

$$\begin{aligned}
A_0 &= \frac{\cosh\alpha'^2}{2\cosh\alpha^2}\left\{\cosh(\eta\alpha^2) + \cos(\eta\alpha^2)\right\},\\
A_1 &= \frac{\sinh\alpha'^2}{2\cosh\alpha^2}\left\{\sinh(\eta\alpha^2) + \sin(\eta\alpha^2)\right\},\\
A_2 &= \frac{\cosh\alpha'^2}{2\cosh\alpha^2}\left\{\cosh(\eta\alpha^2) - \cos(\eta\alpha^2)\right\},\\
A_3 &= \frac{\sinh\alpha'^2}{2\cosh\alpha^2}\left\{\sinh(\eta\alpha^2) - \sin(\eta\alpha^2)\right\},\\
B_0 &= \frac{\cosh\alpha'^2\cosh(\eta\alpha^2)}{\cosh\alpha^2},\\
B_1 &= \frac{\sinh\alpha'^2\sinh(\eta\alpha^2)}{\cosh\alpha^2}.
\end{aligned} \tag{C5}$$

The coefficients $A_0 + A_2 = B_0$ and $A_1 + A_3 = B_1$ represent the probability that the CV qubit resides in the even and odd space, respectively.

When l photons are lost from the CV qubit, the state evolves into $|\psi'_{(l)}\rangle \propto (I \otimes \hat{a}^l)|\psi'_{(0)}\rangle$. Because the state after four-photon subtraction returns to the original state, i.e., $|\psi'_{(4)}\rangle$ and $|\psi'_{(0)}\rangle$ are equivalent up to normalization, the state evolves cyclically into four states with $l = 0, 1, 2, 3$. If a DV photon is lost, we lose the phase information, which results in the mixed state $\tau_{(m)}$, where $m = 0$ (1) if even (odd) photons are lost from the CV qubit.

2. Error analysis

In Sec. A 2, we discuss the X error rate p_X that occurs in B_C for different parities of the input states. Using the weight of the even (odd) parity state after the loss channel, B_0 (B_1), we obtain the failure probability of B_C for noisy input states, written as

$$p'_X(\alpha') = B_0^2 p_{X|\mathrm{EE}}(\alpha') + B_1^2 p_{X|\mathrm{OO}}(\alpha') + 2B_0B_1 p_{X|\mathrm{EO}}(\alpha'). \tag{C6}$$

The X error rate of hybrid fusion becomes $\frac{1}{2}p'_X(\alpha')$ if both DV photons are detected during $B_\mathcal{D}$. That is because we can remove the ambiguity in the Bell measurement once B_I succeeds. If any of the input DV photons are lost, the X error rate is just given by $p'_X(\alpha')$, because we cannot obtain any information from the DV photon. Therefore, the total X error rate of hybrid fusion after loss is written as

$$\begin{aligned}
P_X &= (1-\eta)^2\frac{p'_X(\alpha')}{2} + (2\eta-\eta^2)p'_X(\alpha')\\
&= \frac{1+2\eta-\eta^2}{2}p'_X(\alpha').
\end{aligned} \tag{C7}$$

Phase errors occur due to the photon loss. Let us first assume that l_A photons are lost at CV mode A and that no photon is lost at CV mode C. As discussed in Sec. A 2, no error occurs when $l_A = 0, 1 \pmod 4$ and an unlocatable Z error occurs when $l_A = 2, 3 \pmod 4$, where the modulo 4 is taken due to the cyclic behavior of the cat code. The same analysis can be made if l_C photons are lost at CV mode C and no photon is lost at CV mode A. If photons are lost at both CV modes, by taking the phase shift induced on both modes into consideration, an unlocatable Z error occurs when $l_A + l_C = 2, 3 \pmod 4$. Once we recognize that the input parity is changed to {odd, odd} from the measurement pattern of B_C, we apply a Z gate to correct the phase error. It corrects the error properly when $l_A + l_C = 2 \pmod 4$ but it induces an unwanted error when $l_A + l_C = 0 \pmod 4$. Taking all of this together, the unlocatable Z error rate is written as

$$\begin{aligned}
P_{Z(\mathrm{unloc})} = (1-\eta)^2\big[&2(A_0+A_1)(A_2+A_3)\\
&+ (A_1-A_3)^2 p_{Z|\mathrm{OO}}(\alpha')\big],
\end{aligned} \tag{C8}$$

where the first term $(1-\eta)^2$ represents the fact that neither of the DV photons are lost. On the other hand, if we detect that any of the DV photons are lost, a dephasing error occurs, which is modeled by a locatable Z error with probability $1/2$. The rate of the locatable Z error is written as

$$P_{Z(\mathrm{loc})} = \frac{1}{2}\big[1-(1-\eta)^2\big]. \tag{C9}$$

3. Error propagation by fusion operation

To understand error propagation in the cluster state, we briefly introduce the stabilizer formalism. In typical cluster states, stabilizers are given by the tensor product of

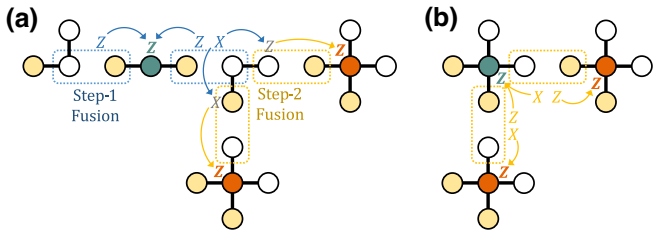

FIG. 7. The propagation of errors from (a) step-1 fusion and (b) step-2 fusion. We only track error propagation resulting in Z errors on data qubits. Note that qubits with Hadamard gates are shaded with yellow.

the Pauli-X operator of a qubit and the Pauli-Z operators of its adjacent qubits. The micro cluster states used in our scheme differ from typical cluster states by Hadamard gates, which exchange the role of the X and Z operators. For example, in the central micro cluster state $|C_3^c\rangle_{102} = H_1H_2|C_3\rangle_{102}$, where Hadamard gates are applied on the side qubits 1 and 2, the stabilizers are given by Z_1Z_0, Z_0Z_2, and $X_1X_0X_2$. If an error occurs on a qubit, it is propagated into adjacent qubits in such a way that the stabilizer statistics are preserved [123]. By following the stabilizer formalism, we find a simple propagation rule for micro cluster states: when a qubit is measured by a fusion operation, the error in the fusion, X or Z, induces the same type of error on its adjacent qubit if the two qubits are in different Hadamard configurations and otherwise, the type of error is changed.

In our simulation, we track only Z errors of data qubits because we only simulate errors on primal lattices and X errors are not detected by Pauli-X measurements. We show error propagation during RHG-lattice construction in Fig. 7. In step 1, two fusion operations are performed, respectively, on the side qubits of $|C_3^c\rangle$. A Z error in the fusion causes a Z error on the data qubit and an X error causes errors on the side qubits of $|C_5^*\rangle$. Errors on the side qubits further propagate to the adjacent data qubits, causing Z errors in the next step. In step 2, a $Z(X)$ error in the fusion propagates, causing a Z error on the data qubit in the direction with (without) the Hadamard gate, following to the propagation rule.

APPENDIX D: SIMULATION DETAILS

1. RHG lattice

Here, we describe the simulation details of the RHG lattice. We perform a Monte Carlo simulation to find the logical error rate and the sequence of each trial is as follows:

(1) We assign the Z error rate to each primal qubit j on the lattice and denote it by $q_{Z,j}$. The error rate includes the propagated one from the fusion operation as well as the Z error due to photon losses.
(2) The errors on qubits are randomly sampled according to the error rate. We determine the value of the syndrome measurement on each cell using the errors of the qubits located on faces of the cell.
(3) The syndromes are decoded to find the error pattern using weighted minimum-weight perfect matching [129] in the PyMatching package [130], where the weight for each qubit is given by $\log\left[(1-q_{Z,j})/q_{Z,j}\right]$.
(4) Once we remove the detected errors, the remaining error chains connect two opposite x boundaries, which are primal. If the number of remaining error chains is odd, we identify a logical error.

By repeating the trial 3×10^5 times, we decide the logical error rate p_L. The logical error rates are calculated with code distances $d = 3, 5$ while varying the loss rate η. The loss threshold η_{th} is obtained by finding the largest η such that p_L decreases with d.

2. Steane code

For circuit-based quantum computation, we simulate a telecorrection circuit of a seven-qubit Steane code with several levels of concatenation. The circuit is composed of the preparation of $|+_L\rangle$, CZ-gate, H-gate, and X-basis measurement. In our simulation, we postselect the successful gate teleportation without error to prevent errors from propagating further. Therefore, only unlocatable errors remain: one is due to photon loss and the other is from the Z error of the fusion operation. In the H-gate teleportation, a Z error of the fusion operation induces an X error on the output qubit because the Hadamard gate is applied on the output qubit. In the CZ-gate teleportation, a Z error of each fusion operation induces a Z error on one of the output qubits. When qubits are stored in quantum memory, photon loss induces a Pauli-Z error.

We find the logical error rate of locatable and unlocatable errors using the Monte Carlo method. In the first level of concatenation, we use the error rates of H-cat qubits with the loss rate η and the amplitude α. The resulting error rates are used for the next level of concatenation. If the error rates tend to decrease for further levels of concatenation, we ensure that error correction works in a fault-tolerant way with the given value of η and α. We repeat the simulation while varying η and α and obtain the loss threshold curve as shown in Fig. 8.

It is shown that the HA scheme achieves a slightly higher threshold than the SDR scheme. However, in the circuit-based error correction, the HA scheme is not efficient because we postselect the successful gate teleportation without error and the located error rate of the HA scheme is of constant order, as shown in Fig. 5. Rather, the SDR scheme is more appropriate due to the near-deterministic success probability of fusion operation.

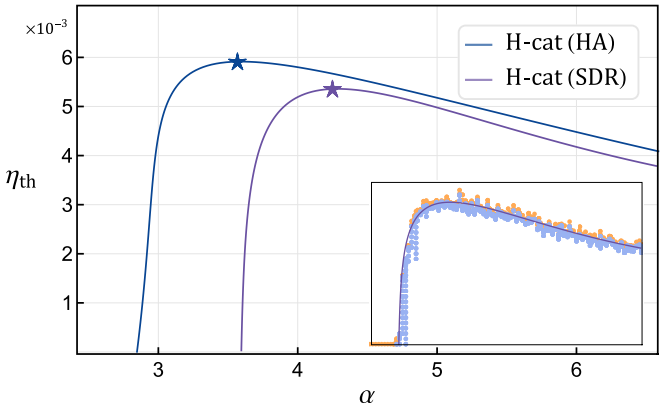

FIG. 8. The threshold curve for the Steane-code simulation with the HA and SDR schemes. Points marked as stars represent the highest loss threshold. In the inset, we present the way of determining the threshold curve. From a Monte Carlo simulation with parameters η and α, we decide if parameters are accepted (rejected) for fault-tolerant computation, which are marked as blue (orange). The threshold curve is determined to be the boundary between two regions.

[1] P. Kok, W. J. Munro, K. Nemoto, T. C. Ralph, J. P. Dowling, and G. J. Milburn, Linear optical quantum computing with photonic qubits, Rev. Mod. Phys. **79**, 135 (2007).

[2] J. L. O'brien, A. Furusawa, and J. Vučković, Photonic quantum technologies, Nat. Photonics **3**, 687 (2009).

[3] S. Slussarenko and G. J. Pryde, Photonic quantum information processing: A concise review, Appl. Phys. Rev. **6**, 041303 (2019).

[4] P. Krantz, M. Kjaergaard, F. Yan, T. P. Orlando, S. Gustavsson, and W. D. Oliver, A quantum engineer's guide to superconducting qubits, Appl. Phys. Rev. **6**, 021318 (2019).

[5] F. Arute, *et al.*, Quantum supremacy using a programmable superconducting processor, Nature **574**, 505 (2019).

[6] Y. Kim, A. Eddins, S. Anand, K. X. Wei, E. van den Berg, S. Rosenblatt, H. Nayfeh, Y. Wu, M. Zaletel, K. Temme, and A. Kandala, Evidence for the utility of quantum computing before fault tolerance, Nature **618**, 500 (2023).

[7] N. Friis, O. Marty, C. Maier, C. Hempel, M. Holzäpfel, P. Jurcevic, M. B. Plenio, M. Huber, C. Roos, R. Blatt, and B. Lanyon, Observation of entangled states of a fully controlled 20-qubit system, Phys. Rev. X **8**, 021012 (2018).

[8] C. D. Bruzewicz, J. Chiaverini, R. McConnell, and J. M. Sage, Trapped-ion quantum computing: Progress and challenges, Appl. Phys. Rev. **6**, 021314 (2019).

[9] M. V. G. Dutt, L. Childress, L. Jiang, E. Togan, J. Maze, F. Jelezko, A. S. Zibrov, P. R. Hemmer, and M. D. Lukin, Quantum register based on individual electronic and nuclear spin qubits in diamond, Science **316**, 1312 (2007).

[10] M. W. Doherty, N. B. Manson, P. Delaney, F. Jelezko, J. Wrachtrup, and L. C. Hollenberg, The nitrogen-vacancy colour centre in diamond, Phys. Rep. **528**, 1 (2013).

[11] S. Pezzagna and J. Meijer, Quantum computer based on color centers in diamond, Appl. Phys. Rev. **8**, 011308 (2021).

[12] J. R. Petta, A. C. Johnson, J. M. Taylor, E. A. Laird, A. Yacoby, M. D. Lukin, C. M. Marcus, M. P. Hanson, and A. C. Gossard, Coherent manipulation of coupled electron spins in semiconductor quantum dots, Science **309**, 2180 (2005).

[13] A. Chatterjee, P. Stevenson, S. De Franceschi, A. Morello, N. P. de Leon, and F. Kuemmeth, Semiconductor qubits in practice, Nat. Rev. Phys. **3**, 157 (2021).

[14] D. E. Browne and T. Rudolph, Resource-efficient linear optical quantum computation, Phys. Rev. Lett. **95**, 010501 (2005).

[15] C. M. Dawson, H. L. Haselgrove, and M. A. Nielsen, Noise thresholds for optical cluster-state quantum computation, Phys. Rev. A **73**, 052306 (2006).

[16] D. A. Herrera-Martí, A. G. Fowler, D. Jennings, and T. Rudolph, Photonic implementation for the topological cluster-state quantum computer, Phys. Rev. A **82**, 032332 (2010).

[17] C. Vigliar, S. Paesani, Y. Ding, J. C. Adcock, J. Wang, S. Morley-Short, D. Bacco, L. K. Oxenløwe, M. G. Thompson, J. G. Rarity, and A. Laing, Error-protected qubits in a silicon photonic chip, Nat. Phys. **17**, 1137 (2021).

[18] S. Bartolucci, P. Birchall, H. Bombín, H. Cable, C. Dawson, M. Gimeno-Segovia, E. Johnston, K. Kieling, N. Nickerson, M. Pant, F. Pastawski, T. Rudolph, and C. Sparrow, Fusion-based quantum computation, Nat. Commun. **14**, 912 (2023).

[19] N. Maring, A. Fyrillas, M. Pont, E. Ivanov, P. Stepanov, N. Margaria, W. Hease, A. Pishchagin, A. Lemaître, I. Sagnes, *et al.*, A versatile single-photon-based quantum computing platform, Nat. Photonics. **18**, 603 (2024).

[20] A. I. Lvovsky, P. Grangier, A. Ourjoumtsev, V. Parigi, M. Sasaki, and R. Tualle-Brouri, Production and applications of non-Gaussian quantum states of light, ArXiv:2006.16985.

[21] P. T. Cochrane, G. J. Milburn, and W. J. Munro, Macroscopically distinct quantum-superposition states as a bosonic code for amplitude damping, Phys. Rev. A **59**, 2631 (1999).

[22] H. Jeong and M. S. Kim, Efficient quantum computation using coherent states, Phys. Rev. A **65**, 042305 (2002).

[23] T. C. Ralph, A. Gilchrist, G. J. Milburn, W. J. Munro, and S. Glancy, Quantum computation with optical coherent states, Phys. Rev. A **68**, 042319 (2003).

[24] S. Yokoyama, R. Ukai, S. C. Armstrong, C. Sornphiphatphong, T. Kaji, S. Suzuki, J.-I. Yoshikawa, H. Yonezawa, N. C. Menicucci, and A. Furusawa, Ultra-large-scale continuous-variable cluster states multiplexed in the time domain, Nat. Photonics **7**, 982 (2013).

[25] A. E. Ulanov, I. A. Fedorov, A. A. Pushkina, Y. V. Kurochkin, T. C. Ralph, and A. I. Lvovsky, Undoing the effect of loss on quantum entanglement, Nat. Photonics **9**, 764 (2015).

[26] M. V. Larsen, X. Guo, C. R. Breum, J. S. Neergaard-Nielsen, and U. L. Andersen, Deterministic generation of a two-dimensional cluster state, Science **366**, 369 (2019).

[27] Y. Zhan and S. Sun, Deterministic generation of loss-tolerant photonic cluster states with a single quantum emitter, Phys. Rev. Lett. **125**, 223601 (2020).

[28] M. V. Larsen, X. Guo, C. R. Breum, J. S. Neergaard-Nielsen, and U. L. Andersen, Deterministic multi-mode gates on a scalable photonic quantum computing platform, Nat. Phys. **17**, 1018 (2021).

[29] S. Takeda, K. Takase, and A. Furusawa, On-demand photonic entanglement synthesizer, Sci. Adv. **5**, eaaw4530 (2019).

[30] Y. Enomoto, K. Yonezu, Y. Mitsuhashi, K. Takase, and S. Takeda, Programmable and sequential Gaussian gates in a loop-based single-mode photonic quantum processor, Sci. Adv. **7**, eabj6624 (2021).

[31] K. Yonezu, Y. Enomoto, T. Yoshida, and S. Takeda, Time-domain universal linear-optical operations for universal quantum information processing, Phys. Rev. Lett. **131**, 040601 (2023).

[32] H.-S. Zhong, *et al.*, Quantum computational advantage using photons, Science **370**, 1460 (2020).

[33] J. M. Arrazola, *et al.*, Quantum circuits with many photons on a programmable nanophotonic chip, Nature **591**, 54 (2021).

[34] L. S. Madsen, F. Laudenbach, M. F. Askarani, F. Rortais, T. Vincent, J. F. F. Bulmer, F. M. Miatto, L. Neuhaus, L. G. Helt, M. J. Collins, A. E. Lita, T. Gerrits, S. W. Nam, V. D. Vaidya, M. Menotti, I. Dhand, Z. Vernon, N. Quesada, and J. Lavoie, Quantum computational advantage with a programmable photonic processor, Nature **606**, 75 (2022).

[35] D. Drahi, D. V. Sychev, K. K. Pirov, E. A. Sazhina, V. A. Novikov, I. A. Walmsley, and A. I. Lvovsky, Entangled resource for interfacing single- and dual-rail optical qubits, Quantum **5**, 416 (2021).

[36] D. Awschalom, *et al.*, Development of quantum interconnects (QuICs) for next-generation information technologies, PRX Quantum **2**, 017002 (2021).

[37] R. Sahu, L. Qiu, W. Hease, G. Arnold, Y. Minoguchi, P. Rabl, and J. M. Fink, Entangling microwaves with light, Science **380**, 718 (2023).

[38] P. van Loock, Optical hybrid approaches to quantum information, Laser Photon. Rev. **5**, 167 (2011).

[39] U. L. Andersen, J. S. Neergaard-Nielsen, P. van Loock, and A. Furusawa, Hybrid discrete- and continuous-variable quantum information, Nat. Phys. **11**, 713 (2015).

[40] K. Park, S.-W. Lee, and H. Jeong, Quantum teleportation between particlelike and fieldlike qubits using hybrid entanglement under decoherence effects, Phys. Rev. A **86**, 062301 (2012).

[41] S.-W. Lee and H. Jeong, Near-deterministic quantum teleportation and resource-efficient quantum computation using linear optics and hybrid qubits, Phys. Rev. A **87**, 022326 (2013).

[42] H. Kwon and H. Jeong, Generation of hybrid entanglement between a single-photon polarization qubit and a coherent state, Phys. Rev. A **91**, 012340 (2015).

[43] H. Jeong, S. Bae, and S. Choi, Quantum teleportation between a single-rail single-photon qubit and a coherent-state qubit using hybrid entanglement under decoherence effects, Quantum Inf. Process. **15**, 913 (2016).

[44] H. Kim, S.-W. Lee, and H. Jeong, Two different types of optical hybrid qubits for teleportation in a lossy environment, Quantum Inf. Process. **15**, 4729 (2016).

[45] H.-K. Lau and M. B. Plenio, Universal quantum computing with arbitrary continuous-variable encoding, Phys. Rev. Lett. **117**, 100501 (2016).

[46] Y. Lim, J. Joo, T. P. Spiller, and H. Jeong, Loss-resilient photonic entanglement swapping using optical hybrid states, Phys. Rev. A **94**, 062337 (2016).

[47] M. Bergmann and P. van Loock, Hybrid quantum repeater for qudits, Phys. Rev. A **99**, 032349 (2019).

[48] K. Huang, H. L. Jeannic, O. Morin, T. Darras, G. Guccione, A. Cavaillès, and J. Laurat, Engineering optical hybrid entanglement between discrete- and continuous-variable states, New J. Phys. **21**, 083033 (2019).

[49] S. Choi, S.-H. Lee, and H. Jeong, Teleportation of a multiphoton qubit using hybrid entanglement with a loss-tolerant carrier qubit, Phys. Rev. A **102**, 012424 (2020).

[50] S. Omkar, Y. S. Teo, and H. Jeong, Resource-efficient topological fault-tolerant quantum computation with hybrid entanglement of light, Phys. Rev. Lett. **125**, 060501 (2020).

[51] S. Omkar, Y. S. Teo, S.-W. Lee, and H. Jeong, Highly photon-loss-tolerant quantum computing using hybrid qubits, Phys. Rev. A **103**, 032602 (2021).

[52] J. Wen, I. Novikova, C. Qian, C. Zhang, and S. Du, Hybrid entanglement between optical discrete polarizations and continuous quadrature variables, Photonics **8**, 552 (2021).

[53] S. Bose and H. Jeong, Quantum teleportation of hybrid qubits and single-photon qubits using Gaussian resources, Phys. Rev. A **105**, 032434 (2022).

[54] S. Takeda, T. Mizuta, M. Fuwa, P. van Loock, and A. Furusawa, Deterministic quantum teleportation of photonic quantum bits by a hybrid technique, Nature **500**, 315 (2013).

[55] H. Jeong, A. Zavatta, M. Kang, S.-W. Lee, L. S. Costanzo, S. Grandi, T. C. Ralph, and M. Bellini, Generation of hybrid entanglement of light, Nat. Photonics **8**, 564 (2014).

[56] O. Morin, K. Huang, J. Liu, H. Le Jeannic, C. Fabre, and J. Laurat, Remote creation of hybrid entanglement between particle-like and wave-like optical qubits, Nat. Photonics **8**, 570 (2014).

[57] A. E. Ulanov, D. Sychev, A. A. Pushkina, I. A. Fedorov, and A. I. Lvovsky, Quantum teleportation between discrete and continuous encodings of an optical qubit, Phys. Rev. Lett. **118**, 160501 (2017).

[58] H. L. Jeannic, A. Cavaillès, J. Raskop, K. Huang, and J. Laurat, Remote preparation of continuous-variable qubits using loss-tolerant hybrid entanglement of light, Optica **5**, 1012 (2018).

[59] D. V. Sychev, A. E. Ulanov, E. S. Tiunov, A. A. Pushkina, A. Kuzhamuratov, V. Novikov, and A. I. Lvovsky, Entanglement and teleportation between polarization and wave-like encodings of an optical qubit, Nat. Commun. **9**, 3672 (2018).

[60] A. Cavaillès, H. Le Jeannic, J. Raskop, G. Guccione, D. Markham, E. Diamanti, M. D. Shaw, V. B. Verma, S. W. Nam, and J. Laurat, Demonstration of Einstein-Podolsky-Rosen steering using hybrid continuous- and discrete-variable entanglement of light, Phys. Rev. Lett. **121**, 170403 (2018).

[61] G. Guccione, T. Darras, H. L. Jeannic, V. B. Verma, S. W. Nam, A. Cavaillès, and J. Laurat, Connecting heterogeneous quantum networks by hybrid entanglement swapping, Sci. Adv. **6**, eaba4508 (2020).

[62] H. C. J. Gan, G. Maslennikov, K.-W. Tseng, C. Nguyen, and D. Matsukevich, Hybrid quantum computing with conditional beam splitter gate in trapped ion system, Phys. Rev. Lett. **124**, 170502 (2020).

[63] T. Darras, B. E. Asenbeck, G. Guccione, A. Cavaillès, H. Le Jeannic, and J. Laurat, A quantum-bit encoding converter, Nat. Photonics **17**, 165 (2023).

[64] M. A. Nielsen and I. L. Chuang, *Quantum Computation and Quantum Information* (Cambridge University Press, Cambridge, 2010).

[65] D. A. Lidar and T. A. Brun, *Quantum Error Correction* (Cambridge University Press, Cambridge, 2013).

[66] D. Gottesman, A. Kitaev, and J. Preskill, Encoding a qubit in an oscillator, Phys. Rev. A **64**, 012310 (2001).

[67] M. H. Michael, M. Silveri, R. T. Brierley, V. V. Albert, J. Salmilehto, L. Jiang, and S. M. Girvin, New class of quantum error-correcting codes for a bosonic mode, Phys. Rev. X **6**, 031006 (2016).

[68] Z. Leghtas, G. Kirchmair, B. Vlastakis, R. J. Schoelkopf, M. H. Devoret, and M. Mirrahimi, Hardware-efficient autonomous quantum memory protection, Phys. Rev. Lett. **111**, 120501 (2013).

[69] M. Mirrahimi, Z. Leghtas, V. V. Albert, S. Touzard, R. J. Schoelkopf, L. Jiang, and M. H. Devoret, Dynamically protected cat-qubits: A new paradigm for universal quantum computation, New J. Phys. **16**, 045014 (2014).

[70] M. Bergmann and P. van Loock, Quantum error correction against photon loss using multicomponent cat states, Phys. Rev. A **94**, 042332 (2016).

[71] L. Li, C.-L. Zou, V. V. Albert, S. Muralidharan, S. M. Girvin, and L. Jiang, Cat codes with optimal decoherence suppression for a lossy bosonic channel, Phys. Rev. Lett. **119**, 030502 (2017).

[72] V. V. Albert, K. Noh, K. Duivenvoorden, D. J. Young, R. T. Brierley, P. Reinhold, C. Vuillot, L. Li, C. Shen, S. M. Girvin, B. M. Terhal, and L. Jiang, Performance and structure of single-mode bosonic codes, Phys. Rev. A **97**, 032346 (2018).

[73] B. M. Terhal, J. Conrad, and C. Vuillot, Towards scalable bosonic quantum error correction, Quantum Sci. Technol. **5**, 043001 (2020).

[74] A. Joshi, K. Noh, and Y. Y. Gao, Quantum information processing with bosonic qubits in circuit QED, Quantum Sci. Technol. **6**, 033001 (2021).

[75] Z. Leghtas, S. Touzard, I. M. Pop, A. Kou, B. Vlastakis, A. Petrenko, K. M. Sliwa, A. Narla, S. Shankar, M. J. Hatridge, M. Reagor, L. Frunzio, R. J. Schoelkopf, M. Mirrahimi, and M. H. Devoret, Confining the state of light to a quantum manifold by engineered two-photon loss, Science **347**, 853 (2015).

[76] N. Ofek, A. Petrenko, R. Heeres, P. Reinhold, Z. Leghtas, B. Vlastakis, Y. Liu, L. Frunzio, S. M. Girvin, L. Jiang, M. Mirrahimi, M. H. Devoret, and R. J. Schoelkopf, Extending the lifetime of a quantum bit with error correction in superconducting circuits, Nature **536**, 441 (2016).

[77] R. Lescanne, M. Villiers, T. Peronnin, A. Sarlette, M. Delbecq, B. Huard, T. Kontos, M. Mirrahimi, and Z. Leghtas, Exponential suppression of bit-flips in a qubit encoded in an oscillator, Nat. Phys. **16**, 509 (2020).

[78] A. Grimm, N. E. Frattini, S. Puri, S. O. Mundhada, S. Touzard, M. Mirrahimi, S. M. Girvin, S. Shankar, and M. H. Devoret, Stabilization and operation of a Kerr-cat qubit, Nature **584**, 205 (2020).

[79] C. Flühmann, T. L. Nguyen, M. Marinelli, V. Negnevitsky, K. Mehta, and J. P. Home, Encoding a qubit in a trapped-ion mechanical oscillator, Nature **566**, 513 (2019).

[80] P. Campagne-Ibarcq, A. Eickbusch, S. Touzard, E. Zalys-Geller, N. E. Frattini, V. V. Sivak, P. Reinhold, S. Puri, S. Shankar, R. J. Schoelkopf, L. Frunzio, M. Mirrahimi, and M. H. Devoret, Quantum error correction of a qubit encoded in grid states of an oscillator, Nature **584**, 368 (2020).

[81] A. Eickbusch, V. Sivak, A. Z. Ding, S. S. Elder, S. R. Jha, J. Venkatraman, B. Royer, S. M. Girvin, R. J. Schoelkopf, and M. H. Devoret, Fast universal control of an oscillator with weak dispersive coupling to a qubit, Nat. Phys. **18**, 1464 (2022).

[82] V. V. Sivak, A. Eickbusch, B. Royer, S. Singh, I. Tsioutsios, S. Ganjam, A. Miano, B. L. Brock, A. Z. Ding, L. Frunzio, S. M. Girvin, R. J. Schoelkopf, and M. H. Devoret, Real-time quantum error correction beyond break-even, Nature **616**, 50 (2023).

[83] S. Konno, W. Asavanant, F. Hanamura, H. Nagayoshi, K. Fukui, A. Sakaguchi, R. Ide, F. China, M. Yabuno, S. Miki, *et al.*, Logical states for fault-tolerant quantum computation with propagating light, Science **383**, 289 (2024).

[84] J. Guillaud and M. Mirrahimi, Repetition cat qubits for fault-tolerant quantum computation, Phys. Rev. X **9**, 041053 (2019).

[85] J. Guillaud and M. Mirrahimi, Error rates and resource overheads of repetition cat qubits, Phys. Rev. A **103**, 042413 (2021).

[86] C. Chamberland, K. Noh, P. Arrangoiz-Arriola, E. T. Campbell, C. T. Hann, J. Iverson, H. Putterman, T. C. Bohdanowicz, S. T. Flammia, A. Keller, G. Refael, J. Preskill, L. Jiang, A. H. Safavi-Naeini, O. Painter, and F. G. Brandão, Building a fault-tolerant quantum computer using concatenated cat codes, PRX Quantum **3**, 010329 (2022).

[87] Z. Ni, S. Li, X. Deng, Y. Cai, L. Zhang, W. Wang, Z.-B. Yang, H. Yu, F. Yan, S. Liu, C.-L. Zou, L. Sun, S.-B. Zheng, Y. Xu, and D. Yu, Beating the break-even point with a discrete-variable-encoded logical qubit, Nature **616**, 56 (2023).

[88] F.-M. L. Régent, C. Berdou, Z. Leghtas, J. Guillaud, and M. Mirrahimi, High-performance repetition cat code using fast noisy operations, Quantum **7**, 1198 (2023).

[89] K. Fukui, A. Tomita, and A. Okamoto, Analog quantum error correction with encoding a qubit into an oscillator, Phys. Rev. Lett. **119**, 180507 (2017).

[90] K. Fukui, A. Tomita, A. Okamoto, and K. Fujii, High-threshold fault-tolerant quantum computation with analog quantum error correction, Phys. Rev. X **8**, 021054 (2018).
[91] A. L. Grimsmo, J. Combes, and B. Q. Baragiola, Quantum computing with rotation-symmetric bosonic codes, Phys. Rev. X **10**, 011058 (2020).
[92] K. Noh and C. Chamberland, Fault-tolerant bosonic quantum error correction with the surface–Gottesman-Kitaev-Preskill code, Phys. Rev. A **101**, 012316 (2020).
[93] M. V. Larsen, C. Chamberland, K. Noh, J. S. Neergaard-Nielsen, and U. L. Andersen, Fault-tolerant continuous-variable measurement-based quantum computation architecture, PRX Quantum **2**, 030325 (2021).
[94] J. E. Bourassa, R. N. Alexander, M. Vasmer, A. Patil, I. Tzitrin, T. Matsuura, D. Su, B. Q. Baragiola, S. Guha, G. Dauphinais, K. K. Sabapathy, N. C. Menicucci, and I. Dhand, Blueprint for a scalable photonic fault-tolerant quantum computer, Quantum **5**, 392 (2021).
[95] I. Tzitrin, T. Matsuura, R. N. Alexander, G. Dauphinais, J. E. Bourassa, K. K. Sabapathy, N. C. Menicucci, and I. Dhand, Fault-tolerant quantum computation with static linear optics, PRX Quantum **2**, 040353 (2021).
[96] K. Noh, C. Chamberland, and F. G. Brandão, Low-overhead fault-tolerant quantum error correction with the surface-GKP code, PRX Quantum **3**, 010315 (2022).
[97] A. Ourjoumtsev, H. Jeong, R. Tualle-Brouri, and P. Grangier, Generation of optical "Schrödinger cats" from photon number states, Nature **448**, 784 (2007).
[98] A. M. Steane, Simple quantum error-correcting codes, Phys. Rev. A **54**, 4741 (1996).
[99] R. Raussendorf, J. Harrington, and K. Goyal, A fault-tolerant one-way quantum computer, Ann. Phys. (NY) **321**, 2242 (2006).
[100] R. Raussendorf, J. Harrington, and K. Goyal, Topological fault-tolerance in cluster state quantum computation, New J. Phys. **9**, 199 (2007).
[101] A. G. Fowler and K. Goyal, Topological cluster state quantum computing, Quant. Info. Comput. **9**, 721 (2009).
[102] A. P. Lund, T. C. Ralph, and H. L. Haselgrove, Fault-tolerant linear optical quantum computing with small-amplitude coherent states, Phys. Rev. Lett. **100**, 030503 (2008).
[103] B. Vlastakis, G. Kirchmair, Z. Leghtas, S. E. Nigg, L. Frunzio, S. M. Girvin, M. Mirrahimi, M. H. Devoret, and R. J. Schoelkopf, Deterministically encoding quantum information using 100-photon Schrödinger cat states, Science **342**, 607 (2013).
[104] C. Wang, Y. Y. Gao, P. Reinhold, R. W. Heeres, N. Ofek, K. Chou, C. Axline, M. Reagor, J. Blumoff, K. M. Sliwa, L. Frunzio, S. M. Girvin, L. Jiang, M. Mirrahimi, M. H. Devoret, and R. J. Schoelkopf, A Schrödinger cat living in two boxes, Science **352**, 1087 (2016).
[105] Z. Wang, Z. Bao, Y. Wu, Y. Li, W. Cai, W. Wang, Y. Ma, T. Cai, X. Han, J. Wang, Y. Song, L. Sun, H. Zhang, and L. Duan, A flying Schrödinger's cat in multipartite entangled states, Sci. Adv. **8**, eabn1778 (2022).
[106] X. L. He, Y. Lu, D. Q. Bao, H. Xue, W. B. Jiang, Z. Wang, A. F. Roudsari, P. Delsing, J. S. Tsai, and Z. R. Lin, Fast generation of Schrödinger cat states using a Kerr-tunable superconducting resonator, Nat. Commun. **14**, 6358 (2023).
[107] X. Pan, J. Schwinger, N.-N. Huang, P. Song, W. Chua, F. Hanamura, A. Joshi, F. Valadares, R. Filip, and Y. Y. Gao, Protecting the quantum interference of cat states by phase-space compression, Phys. Rev. X **13**, 021004 (2023).
[108] C. Monroe, W. C. Campbell, L.-M. Duan, Z.-X. Gong, A. V. Gorshkov, P. W. Hess, R. Islam, K. Kim, N. M. Linke, G. Pagano, P. Richerme, C. Senko, and N. Y. Yao, Programmable quantum simulations of spin systems with trapped ions, Rev. Mod. Phys. **93**, 025001 (2021).
[109] R. W. Heeres, P. Reinhold, N. Ofek, L. Frunzio, L. Jiang, M. H. Devoret, and R. J. Schoelkopf, Implementing a universal gate set on a logical qubit encoded in an oscillator, Nat. Commun. **8**, 94 (2017).
[110] A. Blais, A. L. Grimsmo, S. M. Girvin, and A. Wallraff, Circuit quantum electrodynamics, Rev. Mod. Phys. **93**, 025005 (2021).
[111] C. Monroe, D. M. Meekhof, B. E. King, and D. J. Wineland, A "Schrödinger cat" superposition state of an atom, Science **272**, 1131 (1996).
[112] D. Kienzler, C. Flühmann, V. Negnevitsky, H.-Y. Lo, M. Marinelli, D. Nadlinger, and J. P. Home, Observation of quantum interference between separated mechanical oscillator wave packets, Phys. Rev. Lett. **116**, 140402 (2016).
[113] K. G. Johnson, J. D. Wong-Campos, B. Neyenhuis, J. Mizrahi, and C. Monroe, Ultrafast creation of large Schrödinger cat states of an atom, Nat. Commun. **8**, 697 (2017).
[114] H. Jeon, J. Kang, J. Kim, W. Choi, K. Kim, and T. Kim, Experimental realization of entangled coherent states in two-dimensional harmonic oscillators of a trapped ion, Scientific Reports **14**, 6847 (2024).
[115] J. Hastrup and U. L. Andersen, All-optical cat-code quantum error correction, Phys. Rev. Res. **4**, 043065 (2022).
[116] D. Su, I. Dhand, and T. C. Ralph, Universal quantum computation with optical four-component cat qubits, Phys. Rev. A **106**, 042614 (2022).
[117] J. Hastrup, J. S. Neergaard-Nielsen, and U. L. Andersen, Deterministic generation of a four-component optical cat state, Opt. Lett. **45**, 640 (2020).
[118] R. Raussendorf and H. J. Briegel, A one-way quantum computer, Phys. Rev. Lett. **86**, 5188 (2001).
[119] N. C. Menicucci, P. van Loock, M. Gu, C. Weedbrook, T. C. Ralph, and M. A. Nielsen, Universal quantum computation with continuous-variable cluster states, Phys. Rev. Lett. **97**, 110501 (2006).
[120] D. Gottesman and I. L. Chuang, Demonstrating the viability of universal quantum computation using teleportation and single-qubit operations, Nature **402**, 390 (1999).
[121] N. Lütkenhaus, J. Calsamiglia, and K.-A. Suominen, Bell measurements for teleportation, Phys. Rev. A **59**, 3295 (1999).
[122] J. Calsamiglia and N. Lütkenhaus, Maximum efficiency of a linear-optical Bell-state analyzer, Appl. Phys. B **72**, 67 (2001).
[123] S.-H. Lee, S. Omkar, Y. S. Teo, and H. Jeong, Parity-encoding-based quantum computing with Bayesian error tracking, npj Quantum Inf. **9**, 39 (2023).
[124] S. Omkar, S.-H. Lee, Y. S. Teo, S.-W. Lee, and H. Jeong, All-photonic architecture for scalable quantum computing

with Greenberger-Horne-Zeilinger states, PRX Quantum **3**, 030309 (2022).
[125] J. Cho, Fault-tolerant linear optics quantum computation by error-detecting quantum state transfer, Phys. Rev. A **76**, 042311 (2007).
[126] S.-W. Lee, K. Park, T. C. Ralph, and H. Jeong, Nearly deterministic Bell measurement for multiphoton qubits and its application to quantum information processing, Phys. Rev. Lett. **114**, 113603 (2015).
[127] A. J. F. Hayes, H. L. Haselgrove, A. Gilchrist, and T. C. Ralph, Fault tolerance in parity-state linear optical quantum computing, Phys. Rev. A **82**, 022323 (2010).
[128] E. Knill, Quantum computing with realistically noisy devices, Nature **434**, 39 (2005).
[129] A. G. Fowler, Proof of finite surface code threshold for matching, Phys. Rev. Lett. **109**, 180502 (2012).
[130] O. Higgott, PyMatching: A PYTHON package for decoding quantum codes with minimum-weight perfect matching, ACM Trans. Quantum Comput. **3**, 1 (2022).
[131] H. Jeong, M. S. Kim, and J. Lee, Quantum-information processing for a coherent superposition state via a mixe-dentangled coherent channel, Phys. Rev. A **64**, 052308 (2001).
[132] Y. Chu, P. Kharel, T. Yoon, L. Frunzio, P. T. Rakich, and R. J. Schoelkopf, Creation and control of multi-phonon Fock states in a bulk acoustic-wave resonator, Nature **563**, 666 (2018).
[133] C. T. Hann, C.-L. Zou, Y. Zhang, Y. Chu, R. J. Schoelkopf, S. M. Girvin, and L. Jiang, Hardware-efficient quantum random access memory with hybrid quantum acoustic systems, Phys. Rev. Lett. **123**, 250501 (2019).
[134] M. Bild, M. Fadel, Y. Yang, U. von Lüpke, P. Martin, A. Bruno, and Y. Chu, Schrödinger cat states of a 16-microgram mechanical oscillator, Science **380**, 274 (2023).
[135] S. Touzard, A. Grimm, Z. Leghtas, S. O. Mundhada, P. Reinhold, C. Axline, M. Reagor, K. Chou, J. Blumoff, K. M. Sliwa, S. Shankar, L. Frunzio, R. J. Schoelkopf, M. Mirrahimi, and M. H. Devoret, Coherent oscillations inside a quantum manifold stabilized by dissipation, Phys. Rev. X **8**, 021005 (2018).
[136] J. M. Gertler, S. van Geldern, S. Shirol, L. Jiang, and C. Wang, Experimental realization and characterization of stabilized pair-coherent states, PRX Quantum **4**, 020319 (2023).
[137] S. Puri, S. Boutin, and A. Blais, Engineering the quantum states of light in a Kerr-nonlinear resonator by two-photon driving, npj Quantum Inf. **3**, 18 (2017).
[138] S. Puri, A. Grimm, P. Campagne-Ibarcq, A. Eickbusch, K. Noh, G. Roberts, L. Jiang, M. Mirrahimi, M. H. Devoret, and S. M. Girvin, Stabilized cat in a driven nonlinear cavity: A fault-tolerant error syndrome detector, Phys. Rev. X **9**, 041009 (2019).
[139] S. Puri, L. St-Jean, J. A. Gross, A. Grimm, N. E. Frattini, P. S. Iyer, A. Krishna, S. Touzard, L. Jiang, A. Blais, S. T. Flammia, and S. M. Girvin, Bias-preserving gates with stabilized cat qubits, Sci. Adv. **6**, eaay5901 (2020).
[140] H. Putterman, J. Iverson, Q. Xu, L. Jiang, O. Painter, F. G. S. L. Brandão, and K. Noh, Stabilizing a bosonic qubit using colored dissipation, Phys. Rev. Lett. **128**, 110502 (2022).
[141] L. Gravina, F. Minganti, and V. Savona, Critical Schrödinger cat qubit, PRX Quantum **4**, 020337 (2023).
[142] E. Gouzien, D. Ruiz, F.-M. Le Régent, J. Guillaud, and N. Sangouard, Performance analysis of a repetition cat code architecture: Computing 256-bit elliptic curve logarithm in 9 hours with 126 133 cat qubits, Phys. Rev. Lett. **131**, 040602 (2023).
[143] S. Sagona-Stophel, R. Shahrokhshahi, B. Jordaan, M. Namazi, and E. Figueroa, Conditional π-phase shift of single-photon-level pulses at room temperature, Phys. Rev. Lett. **125**, 243601 (2020).
[144] C. Cui, L. Zhang, and L. Fan, In situ control of effective Kerr nonlinearity with Pockels integrated photonics, Nat. Phys. **18**, 497 (2022).
[145] W. Chen, Y. Lu, S. Zhang, K. Zhang, G. Huang, M. Qiao, X. Su, J. Zhang, J.-N. Zhang, L. Banchi, M. S. Kim, and K. Kim, Scalable and programmable phononic network with trapped ions, Nat. Phys. **19**, 877 (2023).
[146] O. Katz, M. Cetina, and C. Monroe, Programmable *n*-body interactions with trapped ions, PRX Quantum **4**, 030311 (2023).
[147] M. Kudra, M. Kervinen, I. Strandberg, S. Ahmed, M. Scigliuzzo, A. Osman, D. P. Lozano, M. O. Tholén, R. Borgani, D. B. Haviland, G. Ferrini, J. Bylander, A. F. Kockum, F. Quijandría, P. Delsing, and S. Gasparinetti, Robust preparation of Wigner-negative states with optimized snap-displacement sequences, PRX Quantum **3**, 030301 (2022).
[148] N. Kang, *et al.*, in preparation.
[149] D. V. Sychev, A. E. Ulanov, A. A. Pushkina, M. W. Richards, I. A. Fedorov, and A. I. Lvovsky, Enlargement of optical Schrödinger's cat states, Nat. Photonics **11**, 379 (2017).
[150] B. Hacker, S. Welte, S. Daiss, A. Shaukat, S. Ritter, L. Li, and G. Rempe, Deterministic creation of entangled atom-light Schrödinger-cat states, Nat. Photonics **13**, 110 (2019).
[151] A. P. Lund, H. Jeong, T. C. Ralph, and M. S. Kim, Conditional production of superpositions of coherent states with inefficient photon detection, Phys. Rev. A **70**, 020101 (2004).
[152] G. S. Thekkadath, B. A. Bell, I. A. Walmsley, and A. I. Lvovsky, Engineering Schrödinger cat states with a photonic even-parity detector, Quantum **4**, 239 (2020).
[153] K. Takase, J.-i. Yoshikawa, W. Asavanant, M. Endo, and A. Furusawa, Generation of optical Schrödinger cat states by generalized photon subtraction, Phys. Rev. A **103**, 013710 (2021).
[154] Z.-H. Li, Z.-Y. Li, F. Yu, M. Al-Amri, and M. S. Zubairy, Method to deterministically generate large-amplitude optical Schrödinger-cat states, ArXiv:2301.02839.
[155] L. A. Morais, T. Weinhold, M. P. de Almeida, J. Combes, A. Lita, T. Gerrits, S. W. Nam, A. G. White, and G. Gillett, Precisely determining photon-number in real-time, ArXiv:2012.10158.
[156] J. P. Bonilla Ataides, D. K. Tuckett, S. D. Bartlett, S. T. Flammia, and B. J. Brown, The XZZX surface code, Nat. Commun. **12**, 2172 (2021).

[157] A. S. Darmawan, B. J. Brown, A. L. Grimsmo, D. K. Tuckett, and S. Puri, Practical quantum error correction with the XZZX code and Kerr-cat qubits, PRX Quantum **2**, 030345 (2021).

[158] Q. Xu, N. Mannucci, A. Seif, A. Kubica, S. T. Flammia, and L. Jiang, Tailored XZZX codes for biased noise, Phys. Rev. Res. **5**, 013035 (2023).

[159] D. S. Schlegel, F. Minganti, and V. Savona, Quantum error correction using squeezed Schrödinger cat states, Phys. Rev. A **106**, 022431 (2022).

[160] Q. Xu, G. Zheng, Y.-X. Wang, P. Zoller, A. A. Clerk, and L. Jiang, Autonomous quantum error correction and fault-tolerant quantum computation with squeezed cat qubits, npj Quantum Inf. **9**, 78 (2023).

[161] T. Hillmann and F. Quijandría, Quantum error correction with dissipatively stabilized squeezed-cat qubits, Phys. Rev. A **107**, 032423 (2023).

[162] S. J. D. Phoenix, Wave-packet evolution in the damped oscillator, Phys. Rev. A **41**, 5132 (1990).

Correction: Typographical errors in Eqs. (A5), (A6), and (C5) have been fixed.